

1 **Conceptual models of dissolved carbon fluxes in a two-layer**
2 **stratified lake: interannual typhoon responses under extreme**
3 **climates**

4 Hao-Chi Lin¹, Keisuke Nakayama², Jeng-Wei Tsai³, and Chih-Yu Chiu⁴

5

6 ¹ Department of Bioenvironmental Systems Engineering, National Taiwan University,
7 Taipei City, Taiwan

8 ² Graduate School of Engineering, Kobe University, Kobe City, Japan

9 ³ Graduate Institute of Bioresources, National Pingtung University of Science and
10 Technology, Pingtung, Taiwan

11 ⁴ Biodiversity Research Center, Academia Sinica, Taipei City, Taiwan

12

13 * Corresponding author: Keisuke Nakayama (nakayama@phoenix.kobe-u.ac.jp)

14

15 **Abstract**

16 Extreme climates affect the seasonal and interannual patterns of carbon (C) distribution
17 in lentic ecosystems due to the regimes of river inflow and thermal stratification. Typhoons
18 rapidly load substantial amounts of terrestrial C into smaller subtropical lakes (i.e., Yuan-Yang
19 Lake, YYL, Taiwan), renewing and mixing the water column. We developed a conceptual
20 dissolved C model and hypothesized that allochthonous C loading and river inflow intrusion may
21 affect the dissolved inorganic C (DIC) and dissolved organic C (DOC) distributions in a small
22 subtropical lake under these extreme climates. A two-layer conceptual C model was developed to
23 explore how the DIC and DOC fluxes respond to typhoon disturbances on seasonal and
24 interannual time scales in YYL while simultaneously considering autochthonous processes such
25 as algal photosynthesis, remineralization, and vertical transformation. To compare the temporal
26 patterns of fluxes between typhoon years (2015–2016) and non-typhoon years (2017–2018),
27 monthly field samples were obtained and their DIC, DOC, and chlorophyll *a* concentrations
28 measured. The results demonstrated that net ecosystem production was 3.14 times higher in the
29 typhoon years than in the non-typhoon years. This results suggested that a loading of
30 allochthonous C was the most crucial driver of the temporal variation of C fluxes in the typhoon
31 years because of changes in physical and biochemical processes, such as photosynthesis,
32 mineralization, and vertical transportation. However, the lowered vertical transportation rate
33 shaped the seasonal C in the non-typhoon years due to thermal stratification within this small
34 subtropical lake.

35

36 **1. Introduction**

37 The Intergovernmental Panel for Environmental Changes Sixth Assessment Report
38 (IPCC AR6) (2021) suggested that, by 2050, not only is air temperature going to increase by at
39 least about 1.5°C but high-intensity storms and drought events will become more frequent as a
40 result of global warming and climate change. In freshwater ecosystems, extreme climates may
41 change the mixing regimes of freshwater columns (Kraemer et al., 2021; Maberly et al., 2020;
42 Woolway et al., 2020), heat wave events (Woolway et al., 2021a; Woolway et al., 2021b),
43 droughts (Marcé et al., 2019), and floods (Woolway et al., 2018). Freshwater ecosystems store
44 around 0.32 to 1.8 Pg C yr⁻¹, which is approximately equivalent to shallow coastal areas,
45 providing availability to food webs that support human resources, such as acting as processing
46 hotspots in regional carbon (C) cycling (Aufdenkampe et al., 2011; Cole et al., 2007; Engel et
47 al., 2018; Lauerwald et al., 2015; Raymond et al., 2013).

48 The responses of C fluxes in small lakes (lake area < 1 km²) are sensitive to climate
49 change due to the ease with which C mixes within water columns (Doubek et al., 2021;
50 MacIntyre et al., 2021; Winslow et al., 2015). Moreover, storms induce dramatic changes in
51 thermal stratification and water inflows (Lin et al., 2022; Olsson et al., 2022b; Vachon and Del
52 Giorgio, 2014; Woolway et al., 2018). River inflows and wind turbulence released
53 allochthonous C from sediments into the water column after storm events in small stratified
54 lakes (Bartosiewicz et al., 2015; Czikowsky et al., 2018; Vachon and Del Giorgio, 2014). Small
55 lakes account for 25% to 35% of the total area of the earth's surface lakes (Cole et al., 2007;
56 Downing et al., 2006; Raymond et al., 2013). Compared to the case in larger lakes, our
57 understanding of C fluxes in small lakes remain uncertain because small lakes have usually
58 been ignored in calculations of C fluxes on a global scale (Cole et al., 2007; Raymond et al.,
59 2013). Thus, elucidation of the C fluxes in small lakes in extreme weathers conditions is key to
60 optimizing estimations of global C fluxes in extreme climates.

61 Understanding the influences of physical, hydrological, and biogeochemical processes
62 on the fate of C fluxes in smaller lake ecosystems is challenging work (Aufdenkampe et al.,
63 2011; Cole et al., 2007; Raymond et al., 2013; Tranvik et al., 2009; Vachon et al., 2021;
64 Woolway et al., 2018). The physical and biogeochemical regimes under climate change remain
65 uncertain, such as biological compositions, mixing regimes, morphometric characteristics, and
66 air–water energy fluxes (evaporation and transpiration) (Woolway et al., 2020). Dissolved
67 inorganic carbon (DIC) concentration is an important factor in estimating CO₂ fluxes within
68 lake ecosystems (Smith, 1985). Among C fluxes in a freshwater body, the partial pressure of
69 CO₂ (*p*CO₂), defined as CO₂ emission across the air–water interface, is affected by DIC, water
70 temperature, wind speed, and pH (Jähne et al., 1987; Smith, 1985). River inflows, sediment C
71 burial, and heterotrophic respiration in the water column contribute to DIC dynamics in lakes

72 (Hope et al., 2004; Vachon et al., 2021); simultaneously, autotrophic organisms, such as
73 plankton and submerged vegetation, capture DIC via photosynthesis (Amaral et al., 2022;
74 Nakayama et al., 2020; Nakayama et al., 2022). Moreover, calcification and mineralization may
75 consume dissolved oxygen within water, inducing uncertainty in $p\text{CO}_2$ estimation (Hanson et al.,
76 2015; Lin et al., 2022; Nakayama et al., 2022). Dissolved organic carbon (DOC) might
77 contribute to CO_2 emission from lake water to the atmosphere through mineralization and
78 remineralization within lake ecosystems (Hanson et al., 2015; Sobek et al., 2005). In subtropical
79 freshwater ecosystems, DOC concentration is a vital factor in describing variances in
80 mineralization and remineralization rates for dissolved C (Lin et al., 2022; Shih et al., 2019).

81 Typhoons might significantly impact C distributions within the water columns in
82 subtropical regions (Chiu et al., 2020; Lin et al., 2022). Kossin et al. (2013) investigated global
83 storm events with an accumulated rainfall of about 50 mm, which accounts for approximately
84 10 %–40% of precipitation in a subtropical typhoon event. Some studies found not only that
85 extreme rainstorms would impact the dissolved carbon in large lakes and catchments due to
86 weathering (Sun et al., 2021; Zhou et al., 2023) but also that typhoon disturbances quickly mix,
87 renew, or dilute the water in small subtropical lakes (Kimura et al., 2012; Kimura et al., 2017;
88 Lin et al., 2022). However, the complex interactions between biogeochemical and physical
89 regimes for autochthonous and allochthonous C introduce uncertainty in elucidating the
90 complete patterns between typhoons and dissolved C concentrations in small subtropical lakes.
91 This uncertainty hinders our understanding of the seasonal and interannual variations in DIC
92 and DOC concentrations (Lin et al., 2022). Thus, to understand the seasonal regimes and to
93 estimate C fluxes in subtropical lakes, we investigated the variations of DIC and DOC due to
94 typhoon disturbances.

95 Typhoons' effects on C fluxes were previously studied in a small, two-layer stratified,
96 subtropical lake, Yuan–Yang Lake (YYL) in Taiwan (Chiu et al., 2020; Jones et al., 2009; Lin et
97 al., 2021; Lin et al., 2022). Jones et al. (2009) used the conceptual hydrology model and sensor
98 data to estimate CO_2 emission in YYL during typhoon disturbances that occurred in October
99 2004: 2.2 to 2.7 $\text{g C m}^{-2} \text{d}^{-1}$ of CO_2 was released into the atmosphere. CO_2 emissions into the
100 atmosphere were recorded at around 3.0 to 3.7 $\text{g C m}^{-2} \text{d}^{-1}$ in summer and autumn 2015 because
101 of substantial loads of terrestrial C via river inflows after strong typhoons in YYL (Chiu et al.,
102 2020). In particular, vertical mixing, thermal stratification, and river retention regimes were
103 found to be essential physical processes in the C fluxes in YYL (Lin et al., 2021; Lin et al.,
104 2022). The results of these studies suggest that river intrusion and thermal stratification are key
105 factors shaping the seasonal and interannual patterns of C fluxes during typhoon disturbances.
106 River intrusion controls not only the C fluxes, algal biomass, and nutrient loading, but also
107 influences the length of stratification and hydraulic retention times (Lin et al., 2021; Lin et al.,

108 2022; Maranger et al., 2018; Nakayama et al., 2020; Olsson et al., 2022a; Olsson et al., 2022b;
109 Zwart et al., 2017; Vachon and Del Giorgio, 2014). Therefore, we hypothesized that
110 allochthonous C loading and river inflow intrusion might affect DIC and DOC distributions.
111 Further, autochthonous processes in small subtropical lakes, such as algal photosynthesis,
112 remineralization, and vertical transportation, must also be considered. Here, we tested our
113 hypothesis developing two-layer conceptual C models to assess C flux responses to typhoon
114 disturbances in small subtropical lakes.
115

116 **2. Materials and methods**

117 **2.1 Study site**

118 YYL is a shallow (mean water depth: 4.3 m) and oligotrophic (total phosphorous: 10-
119 20 $\mu\text{g-P L}^{-1}$; total nitrogen: 20-60 $\mu\text{g-N L}^{-1}$) subtropical mountain lake (Chou et al., 2000; Tsai
120 et al., 2008; Wu et al., 2001) on Chi-Lan Mountain at around 1,640 asl in north-central Taiwan
121 (24.58° N, 121.40° E) (Fig. 1). Its water is brown because of humic acid content (colored
122 dissolved organic matter: 20–50 ppb QSE; with specific ultraviolet absorbance at 254 nm
123 assessed by a portable fluorometer (model C3; Turner Designs, Sunnyvale, CA, USA); mean
124 pH: 5.4). YYL is surrounded by old-growth trees such as *Chamaecyparis formosensis*,
125 *Chamaecyparis obtusa* var. *formosana*, and *Rhododendron formosanum* Heiml (Chou et al.,
126 2000). Precipitation is over 3,000 mm yr⁻¹, and typhoon precipitation contributes up to half of
127 the total precipitation in YYL annually (Chang et al., 2007; Lai et al., 2006). Due to the rapid
128 renewal of the water body, the water retention time (or residence time) was around 4.4 days in
129 typhoon Megi from 27 September to 1 October 2016 (Lin et al., 2022). The water surface
130 temperature ranges from 15 to 25 °C during March to August, and the water column overturns
131 in September (Kimura et al., 2012; Kimura et al., 2017; Lin et al., 2021). The concentrations of
132 DIC, DOC (Lin et al., 2021), total nitrogen, total phosphate (Chiu et al., 2020; Tsai et al., 2008)
133 and bacteria compositions (Shade et al., 2011) increase within YYL from autumn to winter.
134 YYL has been registered as a long-term ecological study site by the Ministry of Science and
135 Technology (MOST) of Taiwan since 1992 and it became part of the Global Lake Ecological
136 Observatory Network (GLEON) in 2004.
137

138 **2.2 Water sampling and chemical analysis**

139 We collected water quality samples (DOC, DIC, and Chl. *a*) at water depths of 0.04,
140 0.50, 1.00, 2.00, and 3.50 m at the buoy site (Fig. 1). From January 2015 to December 2018, we
141 measured the water surfaces for six river inflows and one outflow each month using a horizontal
142 van Dorn bottle (2.20 L, acrylic) (Fig. 1). These liquid samples were collected using a portable

143 hand pump and glass microfiber filter papers (47 mm GF/F, nominal pore size 0.70 μm ;
144 Whatman, Maidstone, Kent, UK) to obtain filtrate samples. Water samples were stored at
145 around 4°C in a refrigerator until analysis. Samples were analyzed using an infrared gas detector
146 to detect DIC and DOC concentrations with persulfate digestion (model 1088 Rotary TOC
147 autosampler; OI Analytical, College Station, TX, USA). The filter papers were kept refrigerated
148 in opaque bottles at around -25 °C in a refrigerator until the samples were analyzed. In the
149 laboratory, the filter papers were extracted with methanol to obtain Chl. *a* concentration using a
150 portable fluorometer (model 10-AU-005-CE; Turner Designs, Sunnyvale, CA, USA), with
151 specific wavelengths were 430 nm (blue) and 662 nm (red). All analysis was completed within
152 72 hours of exposure to light to reduce the degradation.

153

154 **2.3 Data analysis and numerical modeling**

155 Three water quality variables (DIC, DOC, and Chl. *a*) were compared between different
156 layers (upper and lower layers), years (typhoon and non-typhoon years), and seasons (spring,
157 summer, autumn, and winter). First, we separated our investigation data into typhoon years and
158 non-typhoon years as described in Sect. 2.3.1. Next, to simulate the DIC and DOC concentration
159 under extreme weather scenarios in YYL, we developed a conceptual equations model to generate
160 continuous DIC and DOC data at the upper and lower layers, as shown in Sect. 2.3.2. This also
161 helped us understand the transportation, photosynthesis, and remineralization rates between
162 seasons and between typhoon and non-typhoon years.

163

164 **2.3.1 Typhoon and non-typhoon years**

165 We collected meteorological data from a tower located about 1.0 km from YYL (Lin et
166 al., 2021; Lin et al., 2022). Data on rainfall (model N-68; Nippon Electric Instrument, Tokyo,
167 Japan) and wind speed (model 03001, R.M. Young, Traverse City, MI, USA) were stored in a
168 datalogger (model CR1000; Campbell Scientific, Logan, UT, USA) every 10 min. River discharge
169 (Q_{in} , $\text{m}^3 \text{d}^{-1}$) was estimated every 10 min using the rainfall data and a water depth meter (model
170 HOBO U20; Onset Computer, Bourne, MA, USA) at the end of a river inflow (Fig. 1) using the
171 Manning formula. Transparency was estimated using Secchi disc data measured at a certain
172 interval in that time frame from 10:00 to 14:00 (GMT+08:00).

173

174 As Table 1 shows, four strong typhoons were recorded by using wind speed and rainfall
175 meteorological parameters, contributing a total of 2,254 mm of precipitation in all 24 months of
176 2015 and 2016; this accounted for 35.6% of across two years of typical rainfall ($> 3000 \text{ mm yr}^{-1}$).
177 However, no typhoon rainfall was recorded at YYL in 2017 and 2018; the total precipitation
178 was around $1,398 \text{ mm yr}^{-1}$, below half of average years. The annual average wind speed from
2015 to 2016 was higher by 0.09 m s^{-1} than in 2017 and 2018 (Table 1). Despite no significant

179 difference in average water depth between 2017 and 2018, the average discharge in 2015 and
 180 2016 was higher than 774 m³ d⁻¹ in 2017 and 2018 (Table 1). Thus, we considered 2015 and 2016
 181 as typhoon years and 2017 and 2018 as non-typhoon years.

182

183 **2.3.2 Conceptual two-layer DIC and DOC model**

184 Nakayama et al. (2010) successfully developed a conceptual two-layer dissolved oxygen
 185 model based on strong wind turbulence at Tokyo Bay. Lin et al. (2021) pointed out that thermal
 186 stratification that inhibits vertical C flux between the upper and lower layers in shallow stratified
 187 lakes makes it possible to develop conceptual two-layer C models (Lin et al., 2022; Nakayama et
 188 al., 2022). The phytoplankton and remineralization effects on DIC and DOC fluxes ($dDIC/dt$ and
 189 $dDOC/dt$, mg-C L⁻¹ d⁻¹) were considered in a conceptual two-layer equation model as shown in
 190 Equations 1–4. The fluxes in the upper layer (from the water surface to 2.5 m water depth) were
 191 calculated as follows:

$$V_U \frac{dDIC_U}{dt} = Q_U DIC_R - Q_{out} DIC_U - V_U \alpha_{PU} Chl_U + V_U \alpha_{MU} DOC_U + A_I w_I (DIC_L - DIC_U) \quad (1)$$

$$+ Q_L DIC_L - \frac{A_s F_{CO2}}{C_U} + P a_U$$

$$V_U \frac{dDOC_U}{dt} = Q_U DOC_R - Q_{out} DOC_U - V_U \alpha_{MU} DOC_U + A_I w_I (DOC_L - DOC_U) \quad (2)$$

$$+ Q_L DOC_L + P b_U$$

192 Those in the lower layer (from 2.5 to 4.0 m water depth) were calculated as follows:

$$V_L \frac{dDIC_L}{dt} = Q_L DIC_R - V_L \alpha_{PL} Chl_L + V_L \alpha_{ML} DOC_L + A_I w_I (DIC_U - DIC_L) - Q_L DIC_L \quad (3)$$

$$+ \frac{A_B B F_{DIC}}{C_U} + P a_L$$

$$V_L \frac{dDOC_L}{dt} = Q_L DOC_R - V_L \alpha_{ML} DOC_L + A_I w_I (DOC_U - DOC_L) - Q_L DOC_L + P b_L \quad (4)$$

$$V_{total} = V_U + V_L \quad (5)$$

$$Q_{in} = Q_U + Q_L \quad (6)$$

193 where, as shown in Table 2, total lake volume (V_{total} , 53,544 m³) comprises to the upper layer
 194 (V_U , 45,456 m³) and to the lower layer (V_L , 8,808 m³) (Equation 5), and where the lake surface
 195 area (A_s) is 36,000 m² and the bottom of the lake area (A_B) is 3,520 m². The interface is 2.5 m
 196 vertically, and the interface area (A_I) is 7,264 m² in YYL. The water depth varied from 4.56 to

197 4.66 m during the typhoon period (Chiu et al., 2020; Lin et al., 2022). Therefore, we can assume
 198 that the changes in lake volumes and areas were negligible. The coefficient C_U , with a value of
 199 1000, was used to establish a standard unit for F_{CO_2} ($\text{mg-C m}^{-2} \text{d}^{-1}$), considering the air–water
 200 CO_2 exchange by Fick’s law as follows:

$$F_{CO_2} = k_{CO_2} \cdot K_H (pCO_{2\text{water}} - pCO_{2\text{air}}) \quad (7)$$

201 where k_{CO_2} is the gas transfer velocity from empirical wind speed equations (Cole and Caraco,
 202 1998; Jähne et al., 1987; Smith, 1985; Wanninkhof, 1992). K_H is Henry’s coefficient calculated
 203 by water temperature empirical equations (Plummer and Busenberg, 1982). $pCO_{2\text{air}}$ (μatm) is
 204 the CO_2 partial pressure in the atmosphere using air pressure data (Lin et al., 2021; Lin et al.,
 205 2022), and the atmospheric CO_2 concentration is assumed to be 400 ppm. $pCO_{2\text{water}}$ (μatm) is
 206 the CO_2 partial pressure at the water surface around 0.04 m water depth from water quality data
 207 (temperature, pH, and DIC concentrations). The empirical equation (Cai and Wang, 1998) was
 208 also followed by Lin et al. (2021). F_{CO_2} contributed approximately half of the net ecosystem
 209 production (NEP) across the water surface to the atmosphere in YYL (Lin et al., 2021). Further,
 210 because sediment carbon may be an important flux into shallow subtropical lakes, the sediment
 211 C flux (BF_{DIC} , BF_{DOC} , mg-C L^{-1}) in the lower layer was considered (Lin et al., 2022).

212 We assumed that the river discharge and outflow discharge (Q_{out} , $\text{m}^3 \text{d}^{-1}$) are in a
 213 quasi–steady state ($Q_{in} = Q_{out}$), divided into upper discharge (Q_U , $\text{m}^3 \text{d}^{-1}$) and lower discharge
 214 (Q_L , $\text{m}^3 \text{d}^{-1}$) (Equation 6). Lin et al. (2021) showed that the buoyancy frequencies in YYL were
 215 $0.011 \pm 0.004 \text{ s}^{-1}$, $0.013 \pm 0.004 \text{ s}^{-1}$, $0.006 \pm 0.003 \text{ s}^{-1}$, and $0.007 \pm 0.004 \text{ s}^{-1}$ from spring
 216 (March–May), summer (June–August), autumn (September–November), and winter
 217 (December–February), respectively, inhibiting the vertical profile of DIC mixed due to
 218 stratification. We estimated the percentages of Q_U and Q_L based on the buoyancy frequency
 219 following Lin et al. (2020 and 2022). Q_U values were 75%, 80%, 45%, and 50% of Q_{in} for
 220 spring to winter, and Q_L values were 25%, 20%, 55%, and 50% of Q_{in} (Table 2).

221 Extreme weather events might induce stronger seasonal thermal stratification from
 222 spring to summer and longer overturns from autumn to winter, thereby changing C distribution
 223 and transportation within water bodies (Kraemer et al., 2021; Olsson et al., 2022a; Woolway et
 224 al., 2020). Thus, we attempted to simulate extreme climate scenarios; we shifted the ratio of
 225 Q_{in} for each season and tested the river intrusion hypothesis. We established two extreme
 226 conditions: *Level 1* and *Level 2*. *Level 2* is the more extreme condition: Q_U is 80% (spring),
 227 85% (summer), 50% (autumn), and 50% (winter) of Q_{in} ; Q_L is 20% (spring), 15% (summer),
 228 50% (autumn), and 50% (winter) of Q_{in} . *Level 1* is the condition between the present and the
 229 *Level 2* condition: Q_U is 77% (spring), 82% (summer), 47% (autumn), and 50% (winter) of
 230 Q_{in} ; Q_L is 23% (spring), 18% (summer), 53% (autumn), and 50% (winter) of Q_{in} (Table 2).

231 The contributions of photosynthesis production depended on the chlorophyll *a*

232 concentration (Chl_U , Chl_L , mg L^{-1}) and on the absorption coefficients in the upper layer (α_{PU} , d^{-1})
 233 1) and lower layer (α_{PL} , d^{-1}). The coefficients of DOC remineralization rates in the upper layer
 234 (α_{MU} , d^{-1}) and lower layer (α_{ML} , d^{-1}) were also considered in the conceptual models. The Pa_U ,
 235 Pa_L , Pb_U , and Pb_L are constants in the conceptual models. To obtain unknown values (α_{PU} ,
 236 α_{MU} , α_{PL} , α_{ML} , w_I , BF_{DIC} , BF_{DOC} , Pa_U , Pa_L , Pb_U , and Pb_L), we applied multiple
 237 linear regression analysis. Further, these unknown values were tested by trial and error to obtain
 238 the parameters of the *best-fit* condition (Nakayama et al., 2022). The same parameters of the *best-*
 239 *fit* condition were used to obtain the extreme conditions for *Level 1* and *Level 2*. We used the
 240 coefficient of determination (R^2) and the Nash–Sutcliffe model efficiency coefficient (NSE)
 241 (Nash and Sutcliffe, 1970) to quantify the performance of the equation model with DIC and DOC
 242 sampling data (observation data) for each simulation as follows.

$$NSE = 1 - \frac{\sum_{i=1}^n (Obs_i - Sim_i)^2}{\sum_{i=1}^n (Obs_i - Obs)^2} \quad (8)$$

243 where Obs is observation data of DIC and DOC concentrations, and Sim is best-fit data for
 244 conceptual model.

245

246 **2.3.3 DIC and DOC fluxes**

247 Net ecosystem production was defined as the difference between primary production
 248 and ecological respiration ($NEP = GPP - ER$) due to photosynthesis and respiration via biota
 249 (Dodds and Whiles, 2020). Given that we assumed that the C fluxes were dependent on the river
 250 inflows in YYL (Fig. 1), we estimated the NEP by end-member analysis using the C
 251 concentration of the river inflow and outflow (Lin et al., 2021; Nakayama et al., 2020) by
 252 following Equations 9–12. The upper layer NEP of DIC flux (mg C d^{-1}) was obtained from
 253 Equation 1 as follows:

$$\begin{aligned} \text{Upper flux}_{DIC} &= C_U \alpha_{PU} Chl_U - C_U \alpha_{MU} DOC_U - C_U \frac{A_I w_I (DIC_L - DIC_U)}{V_U} - C_U \frac{Pa_U}{V_U} \\ &= C_U \frac{Q_U DIC_R + Q_L DIC_L - Q_{out} DIC_U}{V_U} - \frac{A_S}{V_U} F_{CO2} \\ &= C_U \frac{1}{t_{rU}} \left(\frac{Q_U}{Q_{in}} DIC_R + \frac{Q_L}{Q_{in}} DIC_L - DIC_U \right) - F_C \\ &\quad t_{rU} = \frac{V_U}{Q_{in}} \end{aligned} \quad (9)$$

254 The upper layer flux of DOC flux ($\text{mg C m}^{-3} \text{d}^{-1}$) was estimated from Equation 2:

$$\begin{aligned}
\text{Upper flux}_{\text{DOC}} &= C_U \alpha_{MU} \text{DOC}_U - C_U \frac{A_I w_I (\text{DOC}_L - \text{DOC}_U)}{V_U} - C_U \frac{P b_U}{V_U} \\
&= C_U \frac{Q_U \text{DOC}_R + Q_L \text{DOC}_L - Q_{out} \text{DOC}_U}{V_U} \\
&= C_U \frac{1}{t_{rU}} \left(\frac{Q_U}{Q_{in}} \text{DOC}_R + \frac{Q_L}{Q_{in}} \text{DOC}_L - \text{DOC}_U \right)
\end{aligned} \tag{10}$$

255

256 The lower layer flux of DIC flux ($\text{mg C m}^{-3} \text{ d}^{-1}$) was estimated from Equation 3:

$$\begin{aligned}
\text{Lower flux}_{\text{DIC}} &= C_U \alpha_{PL} \text{Chl}_L - C_U \alpha_{ML} \text{DOC}_L - C_U \frac{A_I w_I (\text{DIC}_U - \text{DIC}_L)}{V_L} - \frac{A_B B F_{\text{DIC}}}{V_L} \\
&\quad - C_U \frac{P a_L}{V_L} = C_U \frac{Q_L (\text{DIC}_R - \text{DIC}_L)}{V_L} = C_U \frac{1}{t_{rL}} \frac{Q_L}{Q_{in}} (\text{DIC}_R - \text{DIC}_L) \\
&\quad t_{rL} = \frac{V_L}{Q_{in}}
\end{aligned} \tag{11}$$

257

258 The lower layer flux of DOC flux ($\text{mg C m}^{-3} \text{ d}^{-1}$) was estimated from Equation 4:

$$\begin{aligned}
\text{Lower flux}_{\text{DOC}} &= C_U \alpha_{ML} \text{DOC}_L - C_U \frac{A_I w_I (\text{DOC}_U - \text{DOC}_L)}{V_L} - \frac{A_B B F_{\text{DOC}}}{V_L} - C_U \frac{P b_L}{V_L} \\
&= C_U \frac{Q_L (\text{DOC}_R - \text{DOC}_L)}{V_L} = C_U \frac{1}{t_{rL}} \frac{Q_L}{Q_{in}} (\text{DOC}_R - \text{DOC}_L)
\end{aligned} \tag{12}$$

259

260 Thus, the total flux of DIC and that of DOC are:

$$\text{Flux}_{\text{DIC}} = \frac{V_U \text{Upper flux}_{\text{DIC}} + V_L \text{Lower flux}_{\text{DIC}}}{V_{total}} \tag{13}$$

$$\text{Flux}_{\text{DOC}} = \frac{V_U \text{Upper flux}_{\text{DOC}} + V_L \text{Lower flux}_{\text{DOC}}}{V_{total}} \tag{14}$$

261

262 where, F_C is $\frac{A_S}{V_U} F_{CO_2}$ and t_{rU} , t_{rL} are residence times (d) in the upper and lower layers,

263 respectively. These parameters were used for the best-fit condition as shown in Table 2.

264

265 **3. Results**

266 **3.1 Measuring data (monthly DIC, DOC, and Chl. a concentrations) in typhoon** 267 **and non-typhoon years**

268 The comparisons between the two typhoon years (2015 and 2016) revealed no
269 significant differences in DIC, DOC, and Chl *a* concentrations between the upper and lower layers;
270 however, all these parameters differed significantly between the layers in the non-typhoon years
271 2017 and 2018 (Fig. 2). This is because of typhoon-induced mixing and lower thermal
272 stratification between upper and lower layer (Lin et al., 2021; Lin et al., 2022). Overall, the average
273 DIC_U was 2.06 mg-C L⁻¹, and DIC_L was 3.66 mg-C L⁻¹; the average DOC_U was 5.87 mg-C L⁻¹,
274 and DOC_L was 8.02 mg-C L⁻¹; and Chl_U and Chl_L were 2.13 μg-C L⁻¹ and 18.5 μg-C L⁻¹,
275 respectively. In typhoon years, the average DIC_U was 2.34 mg-C L⁻¹, and DIC_L was 4.07 mg-C
276 L⁻¹; the average DOC_U was 6.10 mg-C L⁻¹, and DOC_L was 8.38 mg-C L⁻¹; and the Chl_U and
277 Chl_L were 2.38 μg-C L⁻¹ 12.2 μg-C L⁻¹, respectively (Fig. 2); In non-typhoon years, the average
278 DIC_U was 1.81 mg-C L⁻¹, and DIC_L was 3.28 mg-C L⁻¹; the average DOC_U was 5.66 mg-C L⁻¹,
279 and DOC_L was 7.67 mg-C L⁻¹; and Chl_U and Chl_L were 1.89 μg-C L⁻¹ and 24.4 μg-C L⁻¹,
280 respectively (Fig. 2).

281 ANOVA results indicated no significant differences in DIC concentrations among
282 seasons during the typhoon years (p -values ≥ 0.05), suggesting a lack of statistically significant
283 variation in DIC data across seasons (Fig. 3a–b). However, the DOC concentration showed
284 significant differences between seasons in the typhoon years (Fig. 3c–d). No significant
285 differences between Chl_U and Chl_L were observed among the seasons (Fig. 3e–f), whereas the
286 standard deviations (SD) of DIC and DOC were higher in summer and autumn (Fig. 3) due to
287 terrestrial C loading (Chiu et al., 2020). In summer, the SD values of DIC_U and DOC_U were
288 3.51 mg-C L⁻¹ and 3.69 mg-C L⁻¹, respectively (Fig. 3a, c, e). In autumn, DIC_L and DOC_L had
289 the highest SD (4.06 and 4.17 mg-C L⁻¹, respectively) (Fig. 3b, d). Notably, the maximums of
290 DIC_U and DOC_U were 7.06 and 15.6 mg-C L⁻¹ and those of DIC_L and DOC_L were 10.9 and
291 19.8 mg-C L⁻¹, respectively, in the typhoon years (Fig. 3a–d).

292 Positive Pearson correlations of 0.45 to 0.80 were observed between the DOC and DIC
293 in the typhoon years (Fig. 4a). In the non-typhoon years, the upper layer DIC_L was the only
294 variable correlated negatively with DOC in the upper and lower layers (Fig. 4b). DIC in the lower
295 layer was positively correlated with the Chl_L (Fig. 4) due to the abundant respiration in the lower
296 layer (Lin et al., 2021; Tsai et al., 2008).

297

298 **3.2 Performance of simulation data in conceptual two-layer DIC and DOC**
299 **models**

300 The results for the typhoon years demonstrated that that DIC_U was around 1.5 to 5.0
301 $mg-C L^{-1}$ (Fig. 5a–b) and DIC_L was around 5.0 $mg-C L^{-1}$ (Fig. 5d). In the non-typhoon years
302 (2017–2018), the NSE values of DIC_U and DIC_L were 0.61 and 0.70, respectively. On the other
303 hand, the DOC fit our observation data (R^2 values are 0.91, and 0.46; the NSE coefficients from
304 in equation (8) are 0.95 and 0.73) (Fig. 5c–d, Table 3). The parameters for the conceptual two-
305 layer DIC and DOC models showed different regimes between the typhoon and non-typhoon
306 years (Table 3). In the typhoon years, the photosynthesis absorption rate coefficients (α_{PU} , α_{PL})
307 were negative (photosynthesis < respiration) for each season. YYL was a C source due to a large
308 allochthonous C loading during typhoons; the respiration was elevated by around 30- to 150-fold
309 from summer to autumn. However, the values of the transportation coefficients (w_I) were higher
310 in autumn than in the other seasons (Table 3). Further, the higher remineralization rates during
311 typhoon disturbances from summer to autumn resulted in positive α_{MU} and α_{ML} . In the non-
312 typhoon years, the remineralization rates were negative (Table 3)..

313 We simulated the responses of DIC and DOC to typhoons using conceptual two-layer
314 C models. The results showed that the DIC was more sensitive to typhoon disturbances than
315 DOC under the scenarios of *Level 1* and *Level 2* (Fig.5). Overall, the C level declined in the
316 upper layers but increased in the lower layers (Fig. 5). DIC and DOC in the upper layer tended
317 to decline from 1.0 (*Level 1*) to 2.0 $mg-C L^{-1}$ (*Level 2*) (Fig. 5a, c); however, they increased to
318 10.0 and 20.0 $mg-C L^{-1}$ in the lower layer under *Level 1* and *Level 2*, respectively (Fig. 5b, d).
319 Under extreme weather conditions, *Level 2* usually shifted to different typhoon responses for
320 each season (Fig. S1–S2) due to extreme river intrusions and strengths of thermal stratification
321 (Lin et al., 2021). DIC changes more than DOC under *Level 1* and *Level 2* (Fig. 5) because the
322 photosynthesis, transportation, and remineralization rates may crucially affect the seasonal and
323 interannual patterns of DOC as well.
324

325 3.3 *Interannual responses of NEP to typhoons under extreme weather scenarios*

326 We used filed observation data (Fig 5) to estimate the C fluxes in Table 4. The typhoon
327 disturbances in summer and autumn played an important role in promoting the C released by
328 YYL (Table 4). Overall, YYL released 245 mg C m⁻³ d⁻¹ of DIC and 415 mg C m⁻³ d⁻¹ of DOC
329 during the typhoon years; during the non-typhoon years, it released 51.7 mg C m⁻³ d⁻¹ of DIC
330 and 22.8 mg C m⁻³ d⁻¹ of DOC fluxes (Table 4). The average F_C was 219 and 133 mg C m⁻³ d⁻¹
331 released from YYL into the atmosphere in the typhoon and non-typhoon years, respectively, one
332 to two times larger than Flux_{DIC} (Table 4). In summer, the upper layer exhibited declines in
333 both DIC and DOC concentrations, with DIC being approximately 3.7 times higher in DIC in
334 typhoons than in the non-typhoon years (Table 4). In autumn, 216 mg C d⁻¹ of upper layer DIC
335 was released in the typhoon years, but 46.1 mg C m⁻³ d⁻¹ of upper layer DOC was produced. The
336 upper layer Flux_{DIC} was negative in autumn in the typhoon years when 268 mg C m⁻³ d⁻¹ more
337 F_C was released than in the non-typhoon years. In addition, the lower layer exhibited the largest
338 release of C into the outflow in the typhoon years; however, the flux in the lower layer was
339 more than twice as high in the summer as in the autumn of those years (Table 4). The average
340 total Flux_{DIC} was a release of approximately 3.14 times more C in the typhoon years than in the
341 non-typhoon years. The average total NEP_{DOC} showed an increase of 62.3 mg C m⁻³ d⁻¹ of DOC
342 between the typhoon and non-typhoon years due to the over 10-fold higher flux in the upper
343 layer (Table 4).

344 We compared the fluxes with different model conditions (*Best-fit*, *Level 1*, and *Level*
345 *2*) as shown in Fig. 6, demonstrating that the responses of Flux_{DIC} to typhoons differed
346 dramatically between *Level 1* and *Level 2* (Fig. 6a-c); especially, the Upper Flux_{DIC} released
347 more C in the typhoon years and absorbed more C in the non-typhoon years than *Obs* (Fig. 6a).
348 Not only were the absolute values of Flux_{DIC} over 3 times higher in the typhoon years than in
349 the non-typhoon years (Table 4), but SD was higher in the typhoon years as well (Fig. 6).
350 However, DOC fluxes changed less under *Level 1* and *Level 2* (Fig. 6d-f), a finding that is
351 consistent with our continuous DOC data (Fig. 5c-d).

352 We not only attempted to know the contributions of thermal stratification and river
353 intrusion to DIC and DOC fluxes by using *Level 1* and *Level 2* scenarios in this conceptual model
354 but also the contributions of typhoon disturbances to DIC and DOC fluxes (Fig. 7). We found
355 the DIC and DOC fluxes were both released (Δ Flux_{DIC} and Δ Flux_{DOC}) under *Level 1* and *Level*
356 *2* scenarios (Fig. 7). Typhoon disturbances contributed -102.2, -62.3 mg-C m³ d⁻¹ Flux_{DIC} and
357 Flux_{DOC} in measurements (observation) data (*Obs*), respectively (Fig. 7). The averages of
358 Δ Flux_{DIC} under *Best-fit* was declined 7.0 % (*Level 1*) and 30.0 % (*Level 2*); Δ Flux_{DOC} was
359 declined 56.9 % (*Level 1*) and 118 % (*Level 2*), respectively (Fig. 7).

360 **4. Discussion**

361 **4.1 Biochemical and physical differences of DIC and DOC fluxes between** 362 **typhoon and non-typhoon-years in YYL**

363 The total precipitation was 35.6% higher in the typhoon years than in the non-typhoon
364 years (Table 1). Water retention and typhoon-induced upwelling control the dynamics of DIC
365 and DOC during the summer and autumn (Chiu et al., 2020; Jones et al., 2009; Tsai et al., 2008;
366 Tsai et al., 2011). The absence of typhoon-induced upwelling affected water quality data
367 differences between the upper and lower layers (Chiu et al., 2020; Lin et al., 2022; Tsai et al.,
368 2008; Tsai et al., 2011). DIC, DOC, and Chl. *a* concentrations differed significantly between
369 upper and lower layers in the non-typhoon years (Fig. 2). Further, the abundance of
370 microorganisms leads to intensive respirations in the lower layers during the non-typhoon
371 period in YYL; for example, an anoxic condition at the hypolimnion may decrease the
372 efficiency of C mineralization and remineralization rates in non-typhoon years (Carey et al.,
373 2022; Chiu et al., 2020; Lin et al., 2022; Shade et al., 2010; Shade et al., 2011). Thus, the
374 thermal stratification and anoxic condition may have been controlled by the seasonal and
375 interannual patterns of DIC and DOC fluxes in the non-typhoon years (Tables 3–4; Fig. 5).

376 We found positive correlations significantly between DOC and DIC concentrations in
377 typhoon years (Fig. 4) because substantial amounts of C loading into YYL during the strong
378 typhoon period in 2015 (Fig. 8a–b) due to the last drought year in 2014 (Chiu et al., 2020). Not
379 only the prolonged (or hysteresis) effects might lead to C emissions dramatically in 2015 due to
380 the drought year in 2014 (Chiu et al., 2020), but also the rapid water retention and C loading
381 during strong typhoon periods (Lin et al., 2022) induced vigorous algal biomass production in
382 the lower layer from May to September 2017 (Fig. 8d). Conversely, without the typhoon-
383 induced mixing and refreshing of the water column might be the mineralization dominated the
384 DIC and DOC concentrations in non-typhoon years (Chiu et al., 2020; Hanson et al., 2015; Lin
385 et al., 2022; Vachon et al., 2021), which could result in the positive linear relationship between
386 DIC and DOC concentrations (Fig. 4b, 8a), and negative remineralization rates in non-typhoon
387 years (Table 3). Therefore, these hydraulic, biogeochemical processes and the hysteresis effects
388 might describe different patterns of measurement data between the typhoon years and non-
389 typhoon years.

390 Thermal stratification and allochthonous C loading may drive the responses of fluxes
391 to typhoons in YYL. The absolute values of fluxes were higher in the typhoon years than in the
392 non-typhoon years (Table 4). We found that precipitation from typhoons loaded large amounts
393 of allochthonous C into YYL during summer and autumn, which might explain the higher fluxes
394 in autumn compared to the other seasons (Table 4). Typhoons dramatically changed the seasonal
395 and interannual patterns of DIC fluxes due to river intrusion (Fig. 5a–b; Fig. S1), which proves

396 to our hypothesis and corresponds to the results of previous studies (Chiu et al., 2020; Lin et al.,
397 2021; Lin et al., 2022). In summer, the DOC and DIC concentrations were spatial differences
398 between layers as a “two-layer system” within the water column because the upper and lower
399 layers were inhibited due to strong thermal stratification (Lin et al., 2021; Lin et al., 2022),
400 thereby resulted in the positive upper DIC and DOC fluxes and lower negative upper DIC and
401 DOC fluxes (Table 4).

402 Because of the absence of typhoon-induced mixing and allochthonous C loading, the
403 total fluxes were lower in the non-typhoon years than those in the typhoon years (Table 4). In
404 the typhoon years, our results showed that typhoon-induced upwelling and loading increased by
405 102.2 mg-DIC m⁻³ d⁻¹ and 62.3 mg-DOC m⁻³ d⁻¹ in YYL (Table 4). Additionally, the CO₂
406 emission (F_C) was 43 % higher (~83 mg C m⁻³ d⁻¹) in the typhoon years than in the non-typhoon
407 years (Table 4). Therefore, typhoon disturbances control DIC loading and C emissions in YYL,
408 consistent with our previous studies (Chiu et al., 2020; Lin et al., 2021; Lin et al., 2022).
409 Simultaneously, bio-photochemical mineralization and degradation may play a key role in
410 shaping C fluxes because colored DOC reduces ultraviolet radiation (UVR) and active
411 photosynthetic radiation (PAR) (Allesson et al., 2021; Chiu et al., 2020; Schindler et al., 1996;
412 Scully et al., 1996; Williamson et al., 1999), resulting in the higher light intensity and water
413 temperature in summer consuming 3.7 times more DIC and DOC than in the other seasons
414 (Table 4). These results suggested that the allochthonous C loading and light duration might be
415 the most crucial factor for DIC and DOC fluxes in the typhoon years. Conversely, the
416 transportation rate shaped the seasonal C concentrations due to thermal stratification in the non-
417 typhoon years.

418

419 **4.2 Model limitation under the extreme weather scenarios**

420 Water temperature might be a crucial driver in controlling C fluxes in YYL (Chiu et
421 al., 2020; Lin et al., 2021; Lin et al., 2022). We found that the fluxes and F_{CO_2} in summer were
422 usually higher than in winter (Tables 3–4) due to the higher levels of photosynthesis,
423 remineralization, and thermal stratification strength (Lin et al., 2021; Lin et al., 2022). With the
424 conceptual two-layer C models (Table 3), photosynthesis absorption (α_{PU} , α_{PL}),
425 remineralization (α_{MU} , α_{ML}), and transportation (w_I) well represented the seasonal variations in
426 DIC and DOC data. These parameters of the conceptual two-layer C models appeared in
427 reasonable patterns (Table 3). The higher remineralization and photosynthesis rates resulted in
428 higher absolute values of fluxes in the autumn of the typhoon years (Tables 3–4). In the non-
429 typhoon years, the photosynthesis rates contributed to the total fluxes (Tables 3–4). Thus, the
430 conceptual two-layer C models well characterizes the seasonal and interannual responses of DIC
431 and DOC fluxes to typhoons in YYL.

432 Under the extreme weather events scenarios (*Level 1* and *Level 2*), the DIC and DOC
433 are more released 30 % –118 % within YYL, considering thermal stratification and river
434 intrusion. (Fig. 7). In non-typhoon years, the DIC fluxes were more absorbed than DOC fluxes
435 (Fig. 6) or events for each season (Fig. S1–S2) under extreme weather events scenarios.
436 However, the results showed that the typhoon disturbances that impacted the response of DOC
437 fluxes were more sensitive than DIC fluxes (Fig. 7). In autumn, our results are shown that
438 parameter of transportation rates in typhoon years was over ten-fold higher than non-typhoon
439 years (Table 3), but also DOC concentration was dominated by mineralization in typhoon years
440 (Fig. 8) because biogeochemical processes within lakes, such as respiration, mineralization, and
441 sediment burial, may impact DOC fluxes (Bartosiewicz et al., 2015; Hanson et al., 2015;
442 Maranger et al., 2018). Simultaneously, the physical processes such as typhoon-induced mixing
443 and fall overturns upwelled the sediment and lower layer DOC into the water surface in YYL
444 (Kimura et al. 2017; Lin et al. 2022). Therefore, we suggested that fall overturns and
445 mineralization after typhoon disturbances might be vital in the vertical distribution of DOC
446 concentrations in typhoon years.

447 Ejarque et al. (2021) successfully developed a conceptual one-layer model of DOC
448 and DIC, considering bacterial respiration, photo-mineralization and degradation in a temperate
449 mountain lake. In addition, Nagatomo et al. (2023) suggested that DIC might be underestimated
450 if submerged vegetation is ignored. We suggest that photo-biochemical processes (such as
451 photo-mineralization) and submerged vegetation should be considered in the upper layer to
452 clarify and validate the responses of the total C fluxes under extreme climates in a two-layer
453 stratified lake.

454

455 **5. Conclusions**

456 We successfully developed two-layer conceptual C models to obtain continuous DIC
457 and DOC data in YYL and to simulate extreme conditions. Our conceptual two-layer C model
458 revealed that allochthonous and autochthonous processes both accounted for C flux responses to
459 typhoon disturbances. Without typhoons, thermal stratification was the primary driver of
460 seasonal and interannual patterns of DIC and DOC. In the typhoon years, the changes in
461 seasonal river intrusion regimes in YYL resulted in a 3-fold higher total Flux_{DIC} than in the non-
462 typhoon years. However, our model should be improved for application to extreme climate
463 scenarios by considering other processes within lake, such as sediment burial, photo-
464 degradation processes, and anoxic conditions. The present results suggest that physical
465 processes (river intrusion and vertical transportation) and biogeochemical processes
466 (mineralization, photosynthesis, and respiration) in a subtropical small lake account for the C
467 flux responses to typhoons on seasonal and interannual time scales.
468

469 **Competing interests**

470 The authors have no conflicts of interest to report.

471

472 **Acknowledgements**

473 The authors thank YS Hsueh, LC Jiang, and TY Chen for their help with the water
474 sample collection and chemistry analysis. This work was supported by the Japan Society for the
475 Promotion of Science (JSPS) under grant nos. 22H05726, 22H01601, and 18KK0119 to K
476 Nakayama; and by the Academia Sinica, Taiwan (AS-103-TP-B15), Ministry of Science and
477 Technology, Taiwan (MOST 106-2621-M-239-001, MOST 107-2621-M-239-001, MOST 108-
478 2621-M-239-001) to CY Chiu and JW Tsai. This study benefited from participation in the
479 Global Lakes Ecological Observatory Network (GLEON).

480 Hao-Chi Lin: Conceptualization, Methodology, Investigation, Formal analysis,
481 Writing – original draft. Keisuke Nakayama: Methodology, Supervision, Writing – review &
482 editing, Conceptualization. Jeng-Wei Tsai: Investigation, Funding acquisition, Writing –review
483 & editing. Chih-Yu Chiu: Funding acquisition, Writing – review & editing.

484

485 **Data availability**

486 The data that support the findings of this study are adopted from our previous works,
487 including Chiu et al. (2020), Lin et al. (2021), and Lin et al. (2022).

488

489

490 **References**

- 491 Allesson, L., Koehler, B., Thrane, J.-E., Andersen, T., and Hessen, D. O.: The role of
492 photomineralization for CO₂ emissions in boreal lakes along a gradient of dissolved organic
493 matter, *Limnol. Oceanogr.*, 66, 158–170, <https://doi.org/10.1002/lno.11594>, 2021.
- 494 Amaral, J. H. F., Melack, J. M., Barbosa, P. M., Borges, A. V., Kasper, D., Cortés, A. C., Zhou,
495 W., MacIntyre, S., and Forsberg, B. R.: Inundation, Hydrodynamics and Vegetation
496 Influence Carbon Dioxide Concentrations in Amazon Floodplain Lakes, *Ecosystems*, 25,
497 911–930, <https://doi.org/10.1007/s10021-021-00692-y>, 2022.
- 498 Aufdenkampe, A. K., Mayorga, E., Raymond, P. A., Melack, J. M., Doney, S. C., Alin, S. R.,
499 Aalto, R. E., and Yoo, K.: Riverine coupling of biogeochemical cycles between land,
500 oceans, and atmosphere, *Front. Ecol. Environ.*, 9, 53–60, <https://doi.org/10.1890/100014>,
501 2011.
- 502 Bartosiewicz, M., Laurion, I., and MacIntyre, S.: Greenhouse gas emission and storage in a
503 small shallow lake, *Hydrobiologia*, 757, 101–115, [https://doi.org/10.1007/s10750-015-2240-](https://doi.org/10.1007/s10750-015-2240-2)
504 2, 2015.
- 505 Cai, W.-J. and Wang, Y.: The chemistry, fluxes, and sources of carbon dioxide in the estuarine
506 waters of the Satilla and Altamaha Rivers, Georgia, *Limnol. Oceanogr.*, 43, 657–668,
507 <https://doi.org/10.4319/lo.1998.43.4.0657>, 1998.
- 508 Carey, C. C., Hanson, P. C., Thomas, R. Q., Gerling, A. B., Hounshell, A. G., Lewis, A. S. L.,
509 Lofton, M. E., McClure, R. P., Wander, H. L., Woelmer, W. M., Niederlehner, B. R., and
510 Schreiber, M. E.: Anoxia decreases the magnitude of the carbon, nitrogen, and phosphorus
511 sink in freshwaters, *Glob. Change Biol.*, <https://doi.org/10.1111/gcb.16228>, 2022.
- 512 Chang, S.-C., Wang, C.-P., Feng, C.-M., Rees, R., Hell, U., and Matzner, E.: Soil fluxes of
513 mineral elements and dissolved organic matter following manipulation of leaf litter input in
514 a Taiwan *Chamaecyparis* forest, *For. Ecol. Manag.*, 242, 133–141,
515 <https://doi.org/10.1016/j.foreco.2007.01.025>, 2007.
- 516 Chiu, C.-Y., Jones, J. R., Rusak, J. A., Lin, H.-C., Nakayama, K., Kratz, T. K., Liu, W.-C., Tang,
517 S.-L., and Tsai, J.-W.: Terrestrial loads of dissolved organic matter drive inter-annual carbon
518 flux in subtropical lakes during times of drought, *Sci. Total Environ*, 717, 137052,
519 <https://doi.org/10.1016/j.scitotenv.2020.137052>, 2020.
- 520 Chou, C.-H., Chen, T.-Y., Liao, C.-C., and Peng, C.-I.: Long-term ecological research in the
521 Yuanyang Lake forest ecosystem I. Vegetation composition and analysis, *Bot. Bull. Acad.*
522 *Sin.*, 41, 61–72, 2000.
- 523 Cole, J. J. and Caraco, N. F.: Atmospheric exchange of carbon dioxide in a low-wind

524 oligotrophic lake measured by the addition of SF₆, *Limnol. Oceanogr.*, 43, 647–656,
525 <https://doi.org/10.4319/lo.1998.43.4.0647>, 1998.

526 Cole, J. J., Prairie, Y. T., Caraco, N. F., McDowell, W. H., Tranvik, L. J., Striegl, R. G., Duarte,
527 C. M., Kortelainen, P., Downing, J. A., Middelburg, J. J., and Melack, J.: Plumbing the
528 Global Carbon Cycle: Integrating Inland Waters into the Terrestrial Carbon Budget,
529 *Ecosystems*, 10, 172–185, <https://doi.org/10.1007/s10021-006-9013-8>, 2007.

530 Czikowsky, M. J., MacIntyre, S., Tedford, E. W., Vidal, J., and Miller, S. D.: Effects of Wind
531 and Buoyancy on Carbon Dioxide Distribution and Air-Water Flux of a Stratified Temperate
532 Lake, *J. Geophys. Res. Biogeosci.*, 123, 2305–2322, <https://doi.org/10.1029/2017JG004209>,
533 2018.

534 Dodds, W. K. and Whiles, M. R.: *Freshwater Ecology: Concepts and Environmental*
535 *Applications of Limnology*, Third Edition, Elsevier, United Kingdom, 748-762, 2020.

536 Doubek, J. P., Anneville, O., Dur, G., Lewandowska, A. M., Patil, V. P., Rusak, J. A., Salmaso,
537 N., Seltmann, C. T., Straile, D., Urrutia-Cordero, P., Venail, P., Adrian, R., Alfonso, M. B.,
538 DeGasperi, C. L., Eyto, E., Feuchtmayr, H., Gaiser, E. E., Girdner, S. F., Graham, J. L.,
539 Grossart, H.-P., Hejzlar, J., Jacquet, S., Kirillin, G., Llamas, M. E., Matsuzaki, S.-I. S.,
540 Nodine, E. R., Piccolo, M. C., Pierson, D. C., Rimmer, A., Rudstam, L. G., Sadro, S., Swain,
541 H. M., Thackeray, S. J., Thiery, W., Verburg, P., Zohary, T., and Stockwell, J. D.: The extent
542 and variability of storm-induced temperature changes in lakes measured with long-term and
543 high-frequency data, *Limnol. Oceanogr.*, 66, 1979–1992, <https://doi.org/10.1002/lno.11739>,
544 2021.

545 Douville, H., Raghavan, K., Renwick, J., Allan, R. P., Arias, P. A., Barlow, M., Cerezo-Mota, R.,
546 Cherchi, A., Gan, T. Y., Gergis, J., Jiang, D., Khan, A., Mba, W. P., Rosenfeld, D., Tierney,
547 J., and Zolina, O.: Water cycle changes, Cambridge University Press, *Climate Change 2021:*
548 *The Physical Science Basis. Contribution of Working Group I to 45 the Sixth Assessment*
549 *Report of the Intergovernmental Panel on Climate Change*, 2021.

550 Downing, J. A., Prairie, Y. T., Cole, J. J., Duarte, C. M., Tranvik, L. J., Striegl, R. G.,
551 McDowell, W. H., Kortelainen, P., Caraco, N. F., Melack, J. M., and Middelburg, J. J.: The
552 global abundance and size distribution of lakes, ponds, and impoundments, *Limnol.*
553 *Oceanogr.*, 51, 2388–2397, <https://doi.org/10.4319/lo.2006.51.5.2388>, 2006.

554 Ejarque, E., Scholz, K., Wohlfahrt, G., Battin, T. J., Kainz, M. J., and Schelker, J.: Hydrology
555 controls the carbon mass balance of a mountain lake in the eastern European Alps, *Limnol.*
556 *Oceanogr.*, 66, 2110–2125, <https://doi.org/10.1002/lno.11712>, 2021.

557 Engel, F., Farrell, K. J., McCullough, I. M., Scordo, F., Denfeld, B. A., Dugan, H. A., Eyto, E.
558 de, Hanson, P. C., McClure, R. P., Nöges, P., Nöges, T., Ryder, E., Weathers, K. C., and
559 Weyhenmeyer, G. A.: A lake classification concept for a more accurate global estimate of

560 the dissolved inorganic carbon export from terrestrial ecosystems to inland waters, *Sci. Nat.*,
561 105, 25, <https://doi.org/10.1007/s00114-018-1547-z>, 2018.

562 Hanson, P. C., Pace, M. L., Carpenter, S. R., Cole, J. J., and Stanley, E. H.: Integrating
563 Landscape Carbon Cycling: Research Needs for Resolving Organic Carbon Budgets of
564 Lakes, *Ecosystems*, 18, 363–375, <https://doi.org/10.1007/s10021-014-9826-9>, 2015.

565 Hope, D., Palmer, S. M., Billett, M. F., and Dawson, J. J. C.: Variations in dissolved CO₂ and
566 CH₄ in a first-order stream and catchment: an investigation of soil-stream linkages, *Hydrol.*
567 *Process.*, 18, 3255–3275, <https://doi.org/10.1002/hyp.5657>, 2004.

568 Jähne, B., Münnich, K. O., Bössinger, R., Dutzi, A., Huber, W., and Libner, P.: On the parameters
569 influencing air-water gas exchange, *J. Geophys. Res. Oceans*, 92, 1937,
570 <https://doi.org/10.1029/JC092iC02p01937>, 1987.

571 Jones, S. E., Kratz, T. K., Chiu, C.-Y., and McMahon, K. D.: Influence of typhoons on annual
572 CO₂ flux from a subtropical, humic lake, *Glob. Change Biol.*, 15, 243–254,
573 <https://doi.org/10.1111/j.1365-2486.2008.01723.x>, 2009.

574 Kimura, N., Liu, W.-C., Chiu, C.-Y., and Kratz, T.: The influences of typhoon-induced mixing in
575 a shallow lake, *Lakes Reserv.: Res. Manag.*, 17, 171–183, <https://doi.org/10.1111/j.1440->
576 [1770.2012.00509.x](https://doi.org/10.1111/j.1440-1770.2012.00509.x), 2012.

577 Kimura, N., Liu, W.-C., Tsai, J.-W., Chiu, C.-Y., Kratz, T. K., and Tai, A.: Contribution of
578 extreme meteorological forcing to vertical mixing in a small, shallow subtropical lake, *J.*
579 *Limnol.*, 76, 116–128, <https://doi.org/10.4081/jlimnol.2016.1477>, 2017.

580 Kossin, J. P., Olander, T. L., and Knapp, K. R.: Trend Analysis with a New Global Record of
581 Tropical Cyclone Intensity, *J. Clim.*, 26, 9960–9976, <https://doi.org/10.1175/JCLI-D-13->
582 [00262.1](https://doi.org/10.1175/JCLI-D-13-00262.1), 2013.

583 Kraemer, B. M., Pilla, R. M., Woolway, R. I., Anneville, O., Ban, S., Colom-Montero, W.,
584 Devlin, S. P., Dokulil, M. T., Gaiser, E. E., Hambright, K. D., Hessen, D. O., Higgins, S. N.,
585 Jöhnk, K. D., Keller, W., Knoll, L. B., Leavitt, P. R., Lepori, F., Luger, M. S., Maberly, S. C.,
586 Müller-Navarra, D. C., Paterson, A. M., Pierson, D. C., Richardson, D. C., Rogora, M.,
587 Rusak, J. A., Sadro, S., Salmaso, N., Schmid, M., Silow, E. A., Sommaruga, R., Stelzer, J. A.
588 A., Straile, D., Thiery, W., Timofeyev, M. A., Verburg, P., Weyhenmeyer, G. A., and Adrian,
589 R.: Climate change drives widespread shifts in lake thermal habitat, *Nat. Clim. Chang.*, 11,
590 521–529, <https://doi.org/10.1038/s41558-021-01060-3>, 2021.

591 Lai, I.-L., Chang, S.-C., Lin, P.-H., Chou, C.-H., and Wu, J.-T.: Climatic Characteristics of the
592 Subtropical Mountainous Cloud Forest at the Yuanyang Lake Long-Term Ecological
593 Research Site, Taiwan, *Taiwania*, 51, 317–329, 2006.

594 Lauerwald, R., Laruelle, G. G., Hartmann, J., Ciais, P., and Regnier, P. A.: Spatial patterns in
595 CO₂ evasion from the global river network, *Global Biogeochem. Cycles*, 29, 534–554,

596 <https://doi.org/10.1002/2014GB004941>, 2015.

597 Lin, H.-C., Chiu, C.-Y., Tsai, J.-W., Liu, W.-C., Tada, K., and Nakayama, K.: Influence of
598 Thermal Stratification on Seasonal Net Ecosystem Production and Dissolved Inorganic
599 Carbon in a Shallow Subtropical Lake, *J. Geophys. Res. Biogeosci.*, 126,
600 <https://doi.org/10.1029/2020JG005907>, 2021.

601 Lin, H.-C., Tsai, J.-W., Tada, K., Matsumoto, H., Chiu, C.-Y., and Nakayama, K.: The impacts
602 of the hydraulic retention effect and typhoon disturbance on the carbon flux in shallow
603 subtropical mountain lakes, *Sci. Total Environ*, 803, 150044,
604 <https://doi.org/10.1016/j.scitotenv.2021.150044>, 2022.

605 Maberly, S. C., O'Donnell, R. A., Woolway, R. I., Cutler, M. E. J., Gong, M., Jones, I. D.,
606 Merchant, C. J., Miller, C. A., Politi, E., Scott, E. M., Thackeray, S. J., and Tyler, A. N.:
607 Global lake thermal regions shift under climate change, *Nat Commun.*, 11, 1232,
608 <https://doi.org/10.1038/s41467-020-15108-z>, 2020.

609 MacIntyre, S., Bastviken, D., Arneborg, L., Crowe, A. T., Karlsson, J., Andersson, A., Gålfalk,
610 M., Rutgersson, A., Podgrajsek, E., and Melack, J. M.: Turbulence in a small boreal lake:
611 Consequences for air-water gas exchange, *Limnol. Oceanogr.*, 66, 827–854,
612 <https://doi.org/10.1002/lno.11645>, 2021.

613 Maranger, R., Jones, S. E., and Cotner, J. B.: Stoichiometry of carbon, nitrogen, and phosphorus
614 through the freshwater pipe, *Limnol Oceanogr Lett*, 3, 89–101,
615 <https://doi.org/10.1002/lol2.10080>, 2018.

616 Marcé, R., Obrador, B., Gómez-Gener, L., Catalán, N., Koschorreck, M., Arce, M. I., Singer, G.,
617 and Schiller, D. von: Emissions from dry inland waters are a blind spot in the global carbon
618 cycle, *Earth-Sci. Rev.*, 188, 240–248, <https://doi.org/10.1016/j.earscirev.2018.11.012>, 2019.

619 Nagatomo, K., Nakayama, K., Komai, K., Matsumoto, H., Watanabe, K., Kubo, A., Tada, K.,
620 Maruya, Y., Yano, S., Tsai, J. W., Lin, H. C., Vilas, M., and Hipsey, M. R.: A Spatially
621 Integrated Dissolved Inorganic Carbon (SiDIC) Model for Aquatic Ecosystems Considering
622 Submerged Vegetation, *J Geophys Res Biogeosci*, 128,
623 <https://doi.org/10.1029/2022JG007032>, 2023.

624 Nakayama, K., Kawahara, Y., Kurimoto, Y., Tada, K., Lin, H.-C., Hung, M.-C., Hsueh, M.-L.,
625 and Tsai, J.-W.: Effects of oyster aquaculture on carbon capture and removal in a tropical
626 mangrove lagoon in southwestern Taiwan, *Sci. Total Environ*, 156460,
627 <https://doi.org/10.1016/j.scitotenv.2022.156460>, 2022.

628 Nakayama, K., Komai, K., Tada, K., Lin, H. C., Yajima, H., Yano, S., Hipsey, M. R., and Tsai, J.
629 W.: Modeling dissolved inorganic carbon considering submerged aquatic vegetation, *Ecol.*
630 *Model.*, 431, 109188, <https://doi.org/10.1016/j.ecolmodel.2020.109188>, 2020.

631 Nakayama, K., Sivapalan, M., Sato, C., and Furukawa, K.: Stochastic characterization of the

632 onset of and recovery from hypoxia in Tokyo Bay, Japan: Derived distribution analysis
633 based on “strong wind” events, *Water Resour. Res.*, 46,
634 <https://doi.org/10.1029/2009WR008900>, 2010.

635 Nash, J. E. and Sutcliffe, J. V.: River flow forecasting through conceptual models, I A discussion
636 of principles, *J. Hydrol.*, 10, 398–409, 1970.

637 Olsson, F., Mackay, E. B., Barker, P., Davies, S., Hall, R., Spears, B., Exley, G., Thackeray, S.
638 J., and Jones, I. D.: Can reductions in water residence time be used to disrupt seasonal
639 stratification and control internal loading in a eutrophic monomictic lake?, *J. Environ.*
640 *Manage.*, 304, 114169, <https://doi.org/10.1016/j.jenvman.2021.114169>, 2022a.

641 Olsson, F., Mackay, E. B., Moore, T., Barker, P., Davies, S., Hall, R., Spears, B., Wilkinson, J.,
642 and Jones, I. D.: Annual water residence time effects on thermal structure: A potential lake
643 restoration measure?, *J. Environ. Manage.*, 314, 115082,
644 <https://doi.org/10.1016/j.jenvman.2022.115082>, 2022b.

645 Plummer, L. and Busenberg, E.: The solubilities of calcite, aragonite and vaterite in CO₂-H₂O
646 solutions between 0 and 90°C, and an evaluation of the aqueous model for the system
647 CaCO₃-CO₂-H₂O, *Geochim. Cosmochim. Acta*, 46, 1011–1040,
648 [https://doi.org/10.1016/0016-7037\(82\)90056-4](https://doi.org/10.1016/0016-7037(82)90056-4), 1982.

649 Raymond, P. A., Hartmann, J., Lauerwald, R., Sobek, S., McDonald, C., Hoover, M., Butman,
650 D., Striegl, R., Mayorga, E., Humborg, C., Kortelainen, P., Dürr, H., Meybeck, M., Ciais, P.,
651 and Guth, P.: Global carbon dioxide emissions from inland waters, *Nature*, 503, 355–359,
652 <https://doi.org/10.1038/nature12760>, 2013.

653 Schindler, D. W., Curtis, P. J., Parker, B. R., and Stainton, M. P.: Consequences of climate
654 warming and lake acidification for UV-B penetration in North American boreal lakes,
655 *Nature*, 379, 705–708, <https://doi.org/10.1038/379705a0>, 1996.

656 Scully, N. M., McQueen, D. J., and Lean, D. R. S.: Hydrogen peroxide formation: The
657 interaction of ultraviolet radiation and dissolved organic carbon in lake waters along a 43-
658 75°N gradient, *Limnol. Oceanogr.*, 41, 540–548, <https://doi.org/10.4319/lo.1996.41.3.0540>,
659 1996.

660 Shade, A., Chiu, C.-Y., and McMahon, K. D.: Seasonal and episodic lake mixing stimulate
661 differential planktonic bacterial dynamics, *Microb. Ecol.*, 59, 546–554,
662 <https://doi.org/10.1007/s00248-009-9589-6>, 2010.

663 Shade, A., Read, J. S., Welkie, D. G., Kratz, T. K., Wu, C. H., and McMahon, K. D.: Resistance,
664 resilience and recovery: aquatic bacterial dynamics after water column disturbance, *Environ.*
665 *Microbiol.*, 13, 2752–2767, <https://doi.org/10.1111/j.1462-2920.2011.02546.x>, 2011.

666 Shih, Y.-T., Chen, P.-H., Lee, L.-C., Liao, C.-S., Jien, S.-H., Shiah, F.-K., Lee, T.-Y., Hein, T.,
667 Zehetner, F., Chang, C.-T., and Huang, J.-C.: Dynamic responses of DOC and DIC transport

668 to different flow regimes in a subtropical small mountainous river, *Hydrol. Earth Syst. Sci.*,
669 22, 6579–6590, <https://doi.org/10.5194/hess-22-6579-2018>, 2019.

670 Smith, S. V.: Physical, chemical and biological characteristics* of CO₂ gas flux across the air-
671 water interface, *Plant Cell Environ.*, 8, 387–398, <https://doi.org/10.1111/j.1365-3040.1985.tb01674.x>, 1985.

672
673 Sobek, S., Tranvik, L. J., and Cole, J. J.: Temperature independence of carbon dioxide
674 supersaturation in global lakes, *Global Biogeochem. Cycles*, 19, GB2003,
675 <https://doi.org/10.1029/2004GB002264>, 2005.

676 Sun, P., He, S., Yu, S., Pu, J., Yuan, Y., and Zhang, C.: Dynamics in riverine inorganic and
677 organic carbon based on carbonate weathering coupled with aquatic photosynthesis in a
678 karst catchment, Southwest China, *Water Research*, 189, 116658,
679 <https://doi.org/10.1016/j.watres.2020.116658>, 2021.

680 Tranvik, L. J., Downing, J. A., Cotner, J. B., Loiselle, S. A., Striegl, R. G., Ballatore, T. J.,
681 Dillon, P., Finlay, K., Fortino, K., Knoll, L. B., Kortelainen, P. L., Kutser, T., Larsen, S.,
682 Laurion, I., Leech, D. M., McCallister, S. L., McKnight, D. M., Melack, J. M., Overholt, E.,
683 Porter, J. A., Prairie, Y., Renwick, W. H., Roland, F., Sherman, B. S., Schindler, D. W.,
684 Sobek, S., Tremblay, A., Vanni, M. J., Verschoor, A. M., Wachenfeldt, E. von, and
685 Weyhenmeyer, G. A.: Lakes and reservoirs as regulators of carbon cycling and climate,
686 *Limnol. Oceanogr.*, 54, 2298–2314, https://doi.org/10.4319/lo.2009.54.6_part_2.2298, 2009.

687 Tsai, J.-W., Kratz, T. K., Hanson, P. C., Kimura, N., Liu, W.-C., Lin, F.-P., Chou, H.-M., Wu, J.-
688 T., and Chiu, C.-Y.: Metabolic changes and the resistance and resilience of a subtropical
689 heterotrophic lake to typhoon disturbance, *Can. J. Fish. Aquat. Sci.*, 68, 768–780,
690 <https://doi.org/10.1139/F2011-024>, 2011.

691 Tsai, J.-W., Kratz, T. K., Hanson, P. C., Wu, J.-T., Chang, W. Y. B., Arzberger, P. W., Lin, B.-S.,
692 Lin, F.-P., Chou, H.-M., and Chiu, C.-Y.: Seasonal dynamics, typhoons and the regulation of
693 lake metabolism in a subtropical humic lake, *Freshw. Biol.*, 53, 1929–1941,
694 <https://doi.org/10.1111/j.1365-2427.2008.02017.x>, 2008.

695 Vachon, D. and Del Giorgio, P. A.: Whole-Lake CO₂ Dynamics in Response to Storm Events in
696 Two Morphologically Different Lakes, *Ecosystems*, 17, 1338–1353,
697 <https://doi.org/10.1007/s10021-014-9799-8>, 2014.

698 Vachon, D., Sponseller, R. A., and Karlsson, J.: Integrating carbon emission, accumulation and
699 transport in inland waters to understand their role in the global carbon cycle, *Glob. Change*
700 *Biol.*, 27, 719–727, <https://doi.org/10.1111/gcb.15448>, 2021.

701 Wanninkhof, R.: Relationship between wind speed and gas exchange over the ocean, *J.*
702 *Geophys. Res. Oceans*, 97, 7373, <https://doi.org/10.1029/92JC00188>, 1992.

703 Williamson, C. E., Morris, D. P., Pace, M. L., and Olson, O. G.: Dissolved organic carbon and

704 nutrients as regulators of lake ecosystems: Resurrection of a more integrated paradigm,
705 *Limnol. Oceanogr.*, 44, 795–803, https://doi.org/10.4319/lo.1999.44.3_part_2.0795, 1999.

706 Winslow, L. A., Read, J. S., Hansen, G. J. A., and Hanson, P. C.: Small lakes show muted
707 climate change signal in deepwater temperatures, *Geophys. Res. Lett.*, 42, 355–361,
708 <https://doi.org/10.1002/2014GL062325>, 2015.

709 Woolway, R. I., Anderson, E. J., and Albergel, C.: Rapidly expanding lake heatwaves under
710 climate change, *Environ. Res. Lett.*, 16, 94013, <https://doi.org/10.1088/1748-9326/ac1a3a>,
711 2021a.

712 Woolway, R. I., Jennings, E., Shatwell, T., Golub, M., Pierson, D. C., and Maberly, S. C.: Lake
713 heatwaves under climate change, *Nature*, 589, 402–407, [https://doi.org/10.1038/s41586-020-](https://doi.org/10.1038/s41586-020-03119-1)
714 03119-1, 2021b.

715 Woolway, R. I., Kraemer, B. M., Lenters, J. D., Merchant, C. J., O'Reilly, C. M., and Sharma, S.:
716 Global lake responses to climate change, *Nat. Rev. Earth Environ.*, 1, 388–403,
717 <https://doi.org/10.1038/s43017-020-0067-5>, 2020.

718 Woolway, R. I., Simpson, J. H., Spiby, D., Feuchtmayr, H., Powell, B., and Maberly, S. C.: Physical
719 and chemical impacts of a major storm on a temperate lake: a taste of things to come?, *Climatic*
720 *Change*, 151, 333–347, <https://doi.org/10.1007/s10584-018-2302-3>, 2018.

721 Wu, J.-T., Chang, S.-C., Wang, Y.-S., and Hsu, M.-K.: Characteristics of the acidic environment of
722 the Yuanyang Lake (Taiwan), *Bot. Bull. Acad. Sin.*, 42, 17–22, 2001.

723 Zhou, Y., Yu, X., Zhou, L., Zhang, Y., Xu, H., Zhu, M., Zhu, G., Jang, K.-S., Spencer, R. G. M.,
724 Jeppesen, E., Brookes, J. D., Kothawala, D. N., and Wu, F.: Rainstorms drive export of aromatic
725 and concurrent bio-labile organic matter to a large eutrophic lake and its major tributaries, *Water*
726 *Research*, 229, 119448, <https://doi.org/10.1016/j.watres.2022.119448>, 2023.

727 Zwart, J. A., Sebestyen, S. D., Solomon, C. T., and Jones, S. E.: The Influence of Hydrologic
728 Residence Time on Lake Carbon Cycling Dynamics Following Extreme Precipitation Events,
729 *Ecosystems*, 20, 1000–1014, <https://doi.org/10.1007/s10021-016-0088-6>, 2017.

730

731 **Table 1.** Comparison of Yuan-Yang Lake's rainfall and hydrological records in typhoon and non-
 732 typhoon years.

Records	Typhoon years	Non-typhoon years
Time period (year)	2015-2016	2017-2018
Total precipitation (mm)	6,332	3,795
Total typhoon rainfall (mm)	2,254	0
Annual average wind speed (m s ⁻¹)	1.20	1.11
Average water depth (m ± SD)	4.54 ± 1.7	4.51 ± 1.5
Average river discharge (m ³ d ⁻¹)	3,717	2,943
Transparency (Secchi disc depth, m ± SD)	1.58 ± 0.45	1.38 ± 0.28

733

Table 2. Parameters of the two-layer conceptual model in Yuan-Yang Lake

	Parameters	Value	Unit	
<u>Measurements</u>				
	Q_{out}	Outflow discharge	Daily data	$m^3 d^{-1}$
	Q_{in}	Inflow discharge	Daily data	$m^3 d^{-1}$
	Q_U	Upper layer discharge	Daily data	$m^3 d^{-1}$
	Q_L	Lower layer discharge	Daily data	$m^3 d^{-1}$
	DIC_R	River inflow DIC	Monthly data	$mg-C L^{-1}$
	DIC_U	Upper layer DIC	Monthly data	$mg-C L^{-1}$
	DIC_L	Lower layer DIC	Monthly data	$mg-C L^{-1}$
	Chl_U	Upper layer Chl <i>a</i>	Monthly data	$mg L^{-1}$
	Chl_L	Lower layer Chl <i>a</i>	Monthly data	$mg L^{-1}$
	DOC_U	Upper layer DOC	Monthly data	$mg-C L^{-1}$
	DOC_L	Lower layer DOC	Monthly data	$mg-C L^{-1}$
	F_{CO2}	Carbon emission (equation 7)	Monthly data	$mg-C m^2 d^{-1}$
<u>Constants</u>				
	V_{total}	Total lake volume	53,544	m^3
	V_U	Upper layer volume	45,456	m^3
	V_L	Lower layer volume	8,808	m^3
	A_s	Lake surface area	36,000	m^2
	A_I	Interface area	7,264	m^2
	A_B	Bottom of lake area	3,520	m^2
	C_U	Coefficient of the standard unit	1,000	$L m^{-3}$
<u>Unknow Constants</u>				
	α_{PU}, α_{PL}	Coefficients of photosynthesis	Constant	d^{-1}
	α_{MU}, α_{ML}	Coefficients of mineralization	Constant	d^{-1}
	w_I	Coefficient of vertical transportation	Constant	d^{-1}
	BF_{DIC}, BF_{DOC}	Sediment DIC and DOC emission	Constant	$mg-C L^{-1}$
	Pa_U, Pb_L	Equations constant at lower layer	Constant	$mg m^{-3} d^{-1}$
<u>Extreme scenarios</u>				
		Q_U	Q_L	
		75% (spring),	25% (spring),	
	Q_U and Q_L are followed buoyancy	80% (summer),	20% (summer),	
	frequency for each season (Lin et al.	45% (autumn),	55% (autumn),	
	2021)	50% (winter)	50% (winter)	
<i>Best-fit</i>		of Q_{in}	of Q_{in} .	

<i>Level 1</i>	Best-fit scenario but change upper- and lower-layers discharges (Q_U, Q_L)	77% (spring),	23% (spring),
		82% (summer),	18% (summer),
<i>Level 2</i>	Best-fit scenario but change upper and lower layers discharges (Q_U, Q_L)	47% (autumn),	53% (autumn),
		50% (winter)	50% (winter)
		of Q_{in}	of Q_{in} .
		80% (spring),	20% (spring),
		85% (summer),	15% (summer),
		50% (autumn),	50% (autumn),
		50% (winter)	50% (winter)
		of Q_{in}	of Q_{in} .

735

736 **Table 3.** Best-fit parameters of a two-layer conceptual model of DIC and DOC in Yuan-Yang
 737 Lake from 2015 to 2018.

	2015–2016				2017–2018			
	Typhoon years				Non-typhoon years			
	Spring	Summer	Autumn	Winter	Spring	Summer	Autumn	Winter
<i>Upper layer</i>								
F_{CO_2} (mg-C m ² d ⁻¹)	291	245	422	127	231	143	104	175
α_{PU} (d ⁻¹)	-1.20	-33.1	-183.5	-29.1	8.0	6.0	30.0	7.77
α_{MU} (d ⁻¹)	-0.0227	0.0203	0.08	-0.031	-0.01	-0.039	-0.033	-0.195
w_I (d ⁻¹)	0.230	0.172	1.38	0.30	0.10	0.0478	0.120	0.180
Pa_U (d ⁻¹)	12560	-1317	-23750	9597	9880	14000	17600	10100
Pb_U (d ⁻¹)	-21930	9461	-42130	-17070	-3630	-1251	-20820	-9289
$dDIC_U$ (R ² , NSE)					0.305, 0.614			
$dDOC_U$ (R ² , NSE)					0.909, 0.953			
<i>Lower layer</i>								
α_{PL} (d ⁻¹)	-0.627	-22.1	15.0	-0.878	1.49	-6.87	6.0	-16.6
α_{ML} (d ⁻¹)	-0.025	0.123	0.0755	0.00973	-0.010	-0.0376	-0.04	-0.048
Pa_L (d ⁻¹)	100	-5662	-10500	-1013	151.6	2032	1216	909
Pb_L (d ⁻¹)	-6012	-7395	-53940	-9639	-1338	-6296	-19470	-8748
BF_{DIC} , BF_{DOC} (mg-C L ⁻¹)					0.04, 0.00			
$dDIC_L$ (R ² , NSE)					0.452, 0.707			
$dDOC_L$ (R ² , NSE)					0.460, 0.728			

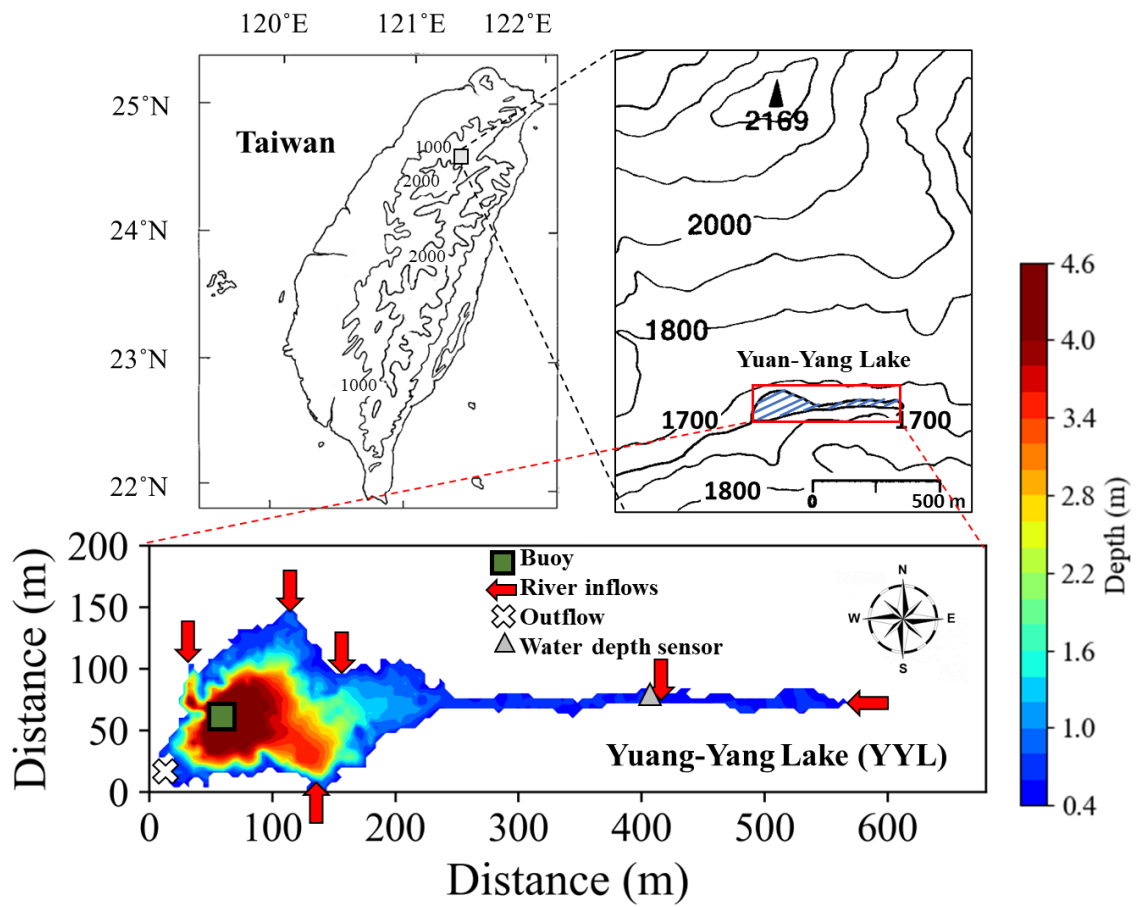
738

739 **Table 4.** Seasonal averages of carbon fluxes ($\text{mg C m}^{-3} \text{ d}^{-1}$) for each season in Yuan-Yang Lake.
740 Positive values are shown in the carbon sink, and negative ones show the values after carbon was
741 released. F_C was carbon emission across water to air by using empirical equations method (Lin
742 et al.2021).

		Flux ($\text{mg C m}^{-3} \text{ d}^{-1}$)			Total ($\text{mg C m}^{-3} \text{ d}^{-1}$)	
		F_C	Upper	Lower	Flux _{DIC}	Flux _{DOC}
<i>Typhoon years</i>	Average	-219	-	-	-150	-9.69
Spring	DIC	-231	-243	-45.2	-210	62.1
	DOC	-	70.8	17.2		
Summer	DIC	-194	29.1	-313	-26.4	18.8
	DOC	-	118	-495		
Autumn	DIC	-351	-216	-659	-288	-151
	DOC	-	46.1	-1167		
Winter	DIC	-100	-96.4	36.5	-74.8	31.2
	DOC	-	40.5	-16.9		
<i>Non-typhoon years</i>	Average	-133	-	-	-47.8	52.6
Spring	DIC	-129	-180	-94.9	-166	-7.06
	DOC	-	21.4	-67.1		
Summer	DIC	-183	5.80	-58.1	-4.57	73.8
	DOC	-	115	-140		
Autumn	DIC	-82.6	95.0	35.9	85.5	95.9
	DOC	-	168	-272		
Winter	DIC	-138	-128	6.04	-106	33.7
	DOC	-	34.0	32.1		

743

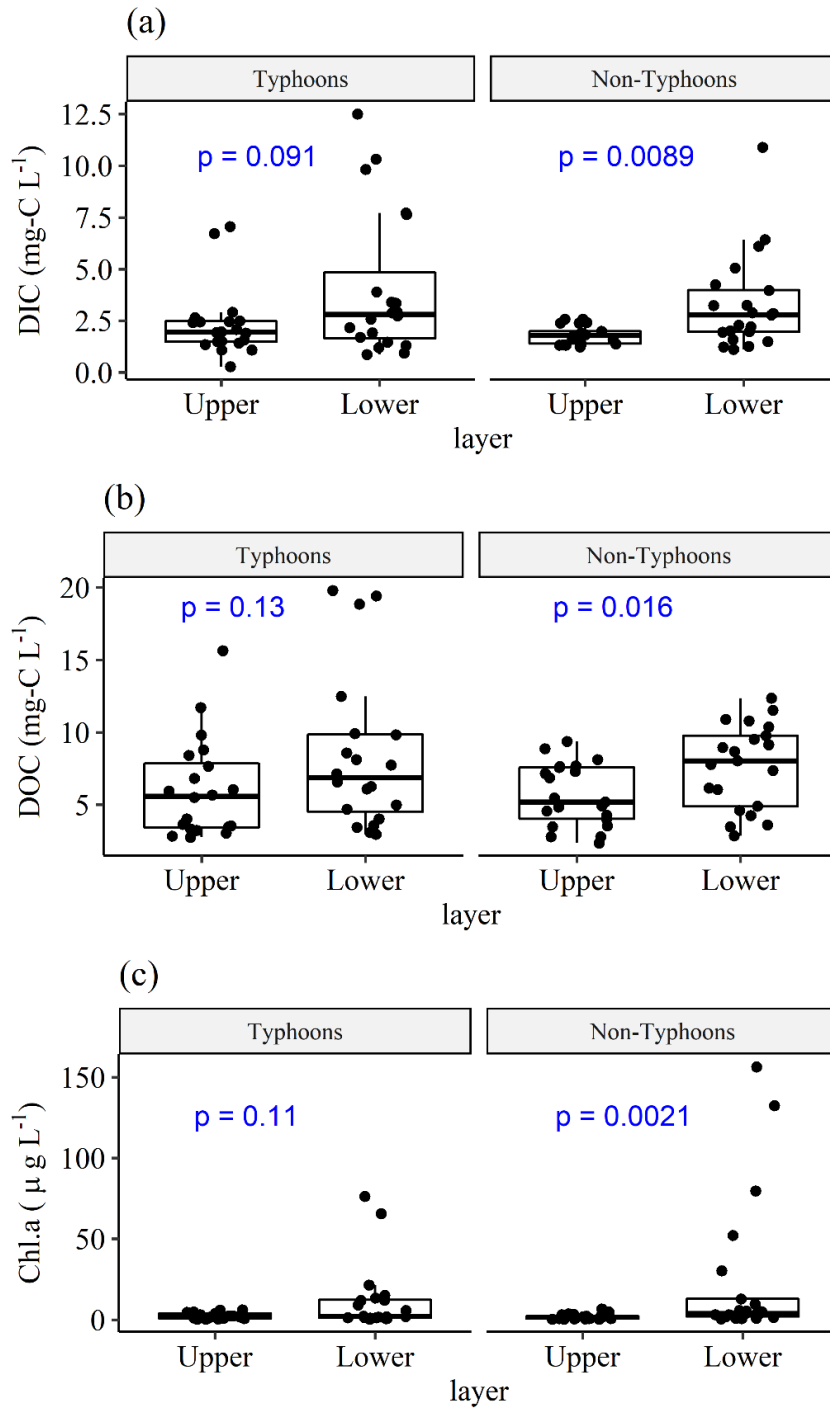
744



745

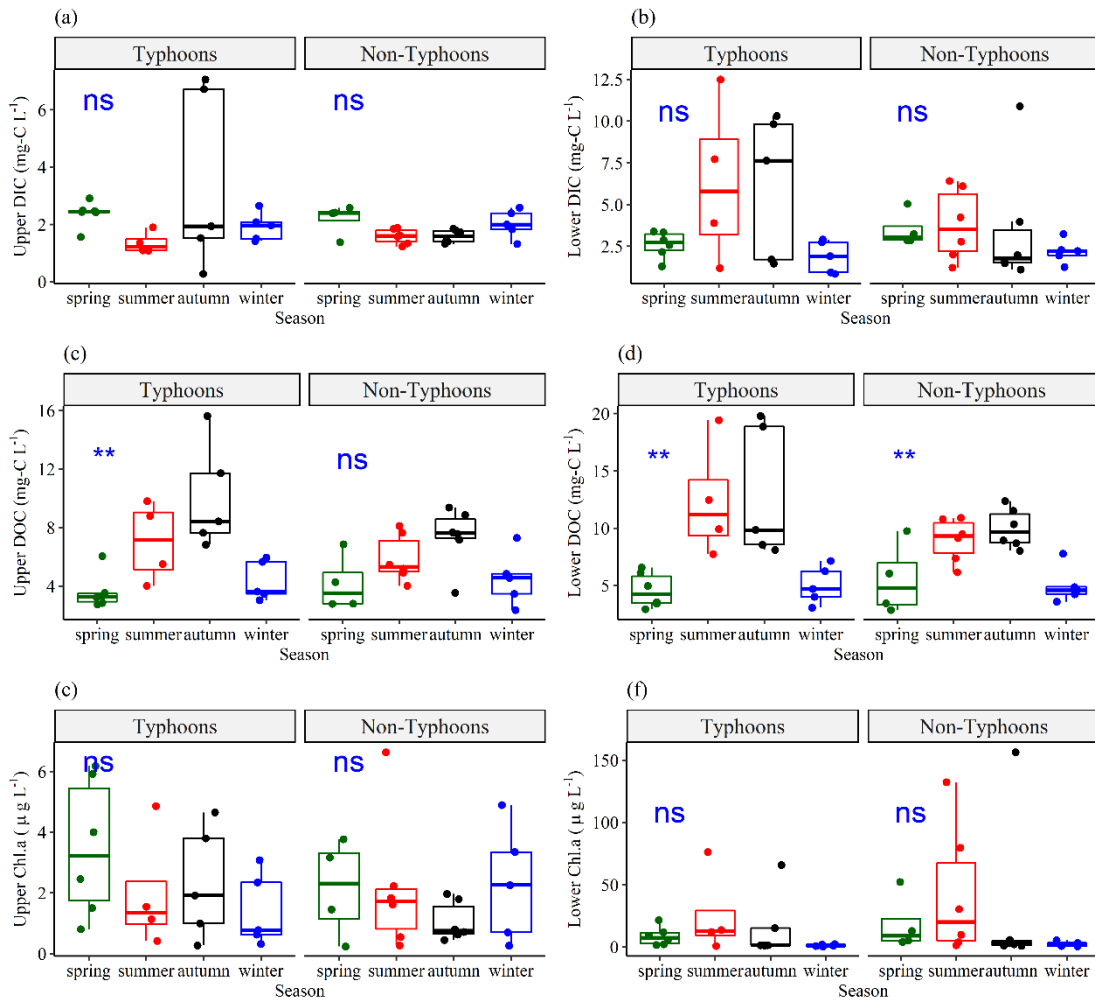
746 **Fig. 1.** Sampling locations and bathymetry maps of Yuan–Yang Lake (YYL). The dark
 747 green rectangle shows the buoy station, which is located at the deepest site of the lake.
 748 The *red points* and *white cross* show the river mouths of the inflows and outflows,
 749 respectively. The *gray triangle* shows the location of the water depth sensor.

750



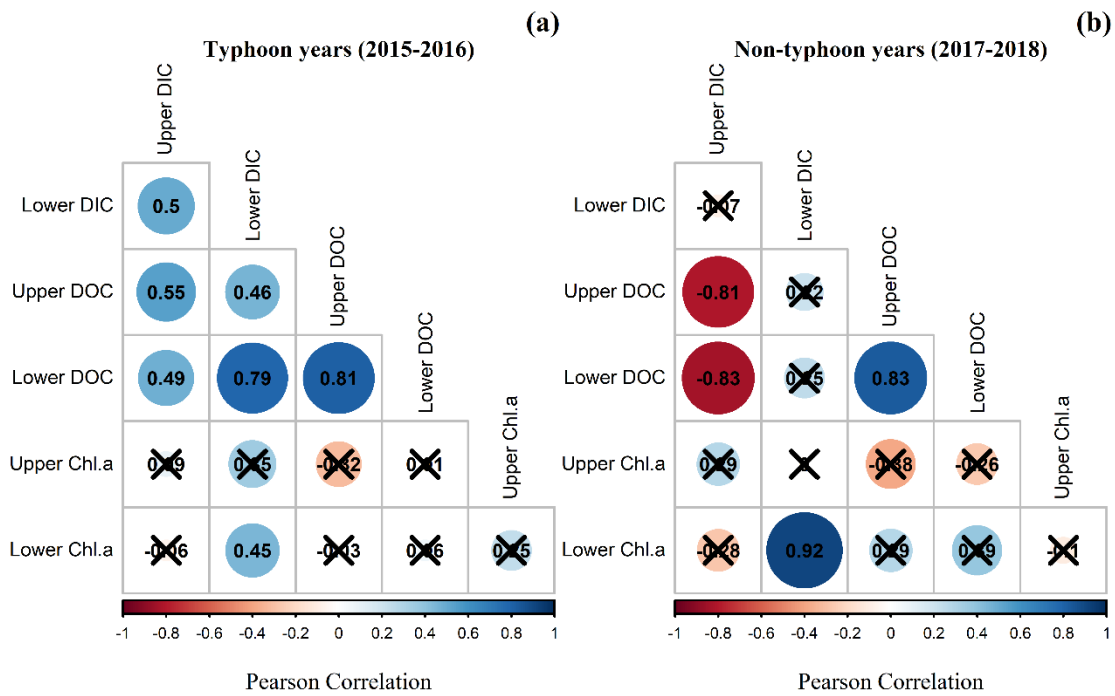
751

752 **Fig. 2.** Comparisons of **(a)** DIC, **(b)** DOC, and **(c)** Chl *a* between upper (DIC_U , DOC_U ,
753 Chl_U) and lower (DIC_L , DOC_L , Chl_L) layers, grouped by typhoon and non-typhoon
754 years. *Bullet points* show the water sampling data. We used a t-test to obtain the *p*-
755 values (*blue texts*). Total sampling numbers are 41 ($n = 41$) for each measurement from
756 January 2015 to December 2018; $n = 20$ in typhoon years, and $n = 21$ in non-typhoon
757 years.



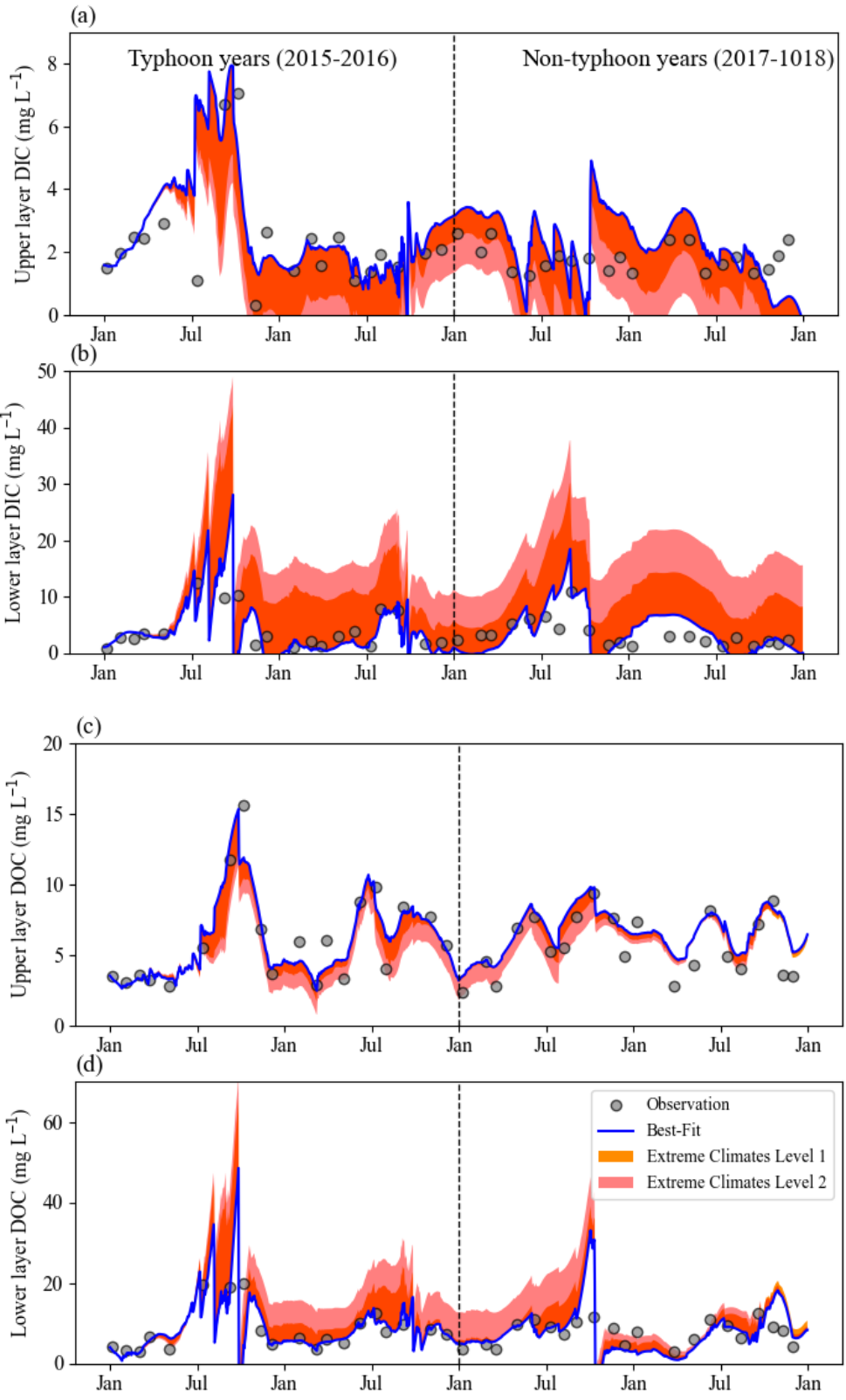
758
 759
 760
 761
 762
 763
 764
 765

Fig. 3. Seasonal variations of (a) upper layer DIC (DIC_U), (b) lower layer DIC (DIC_L), (c) upper layer DOC (DOC_U), (d) lower layer DOC (DOC_L), (e) upper layer Chl. a (Chl_U), (f) lower layer Chl. a (Chl_L) grouped by typhoon and non-typhoon years. The bullet points show the water sampling data. To determine seasonality, we used one-way ANOVA to obtain the p -values. “ns”: p -values ≥ 0.05 ; * show p -values from 0.05 to 0.01; **: p -values from 0.01 to 0.001.



766

767 **Fig. 4.** Pearson correlation coefficients of DIC, DOC, and Chl. *a* concentration at upper
 768 layer and lower layer DIC (DIC_U , DIC_L), DOC (DOC_U , DOC_L), Chl. *a* (Chl_U , Chl_L)
 769 during **(a)** typhoon years and **(b)** non-typhoon years. *Black-crosses* show insignificant
 770 values (p -values are > 0.05).
 771



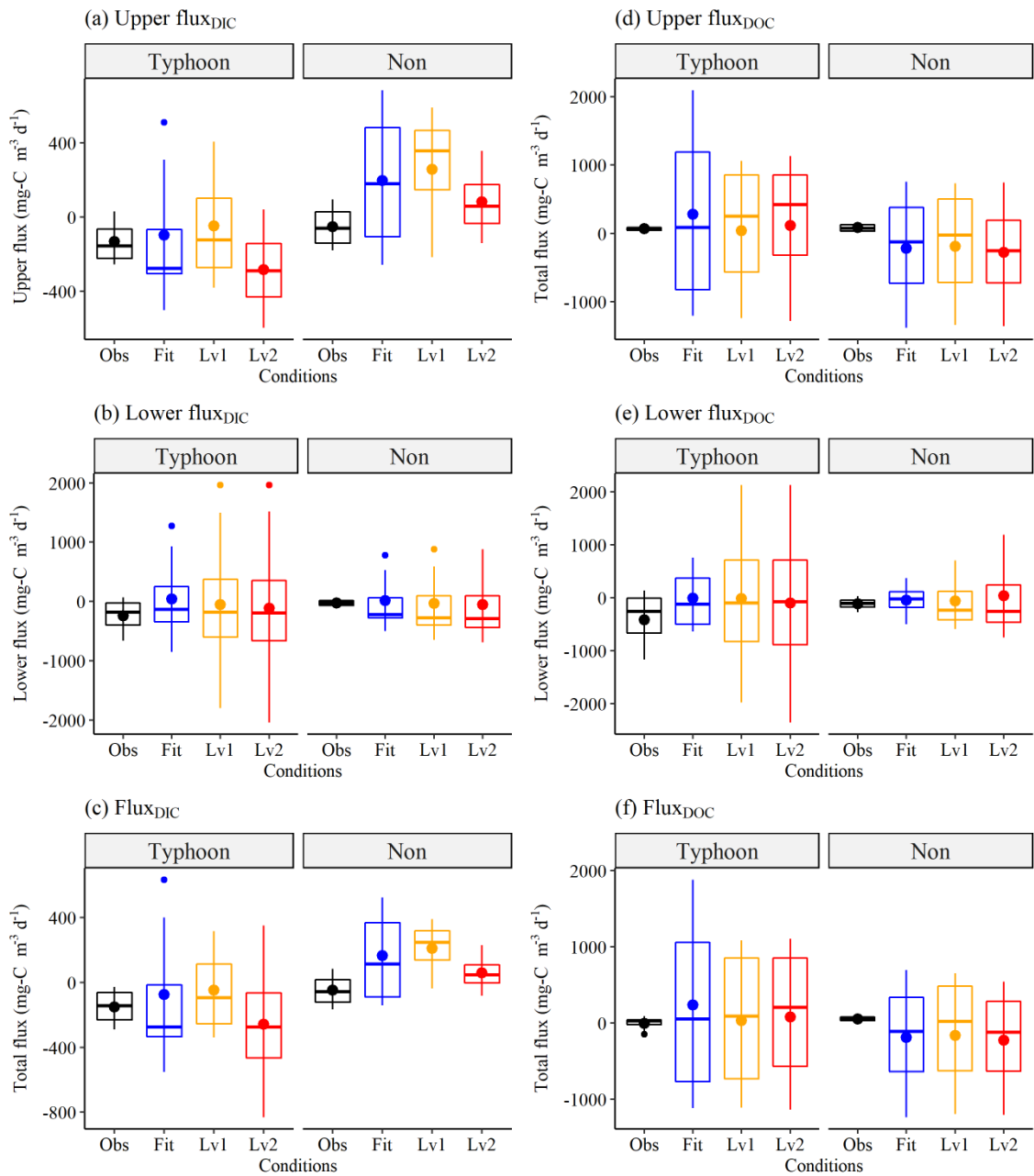
772

773

774

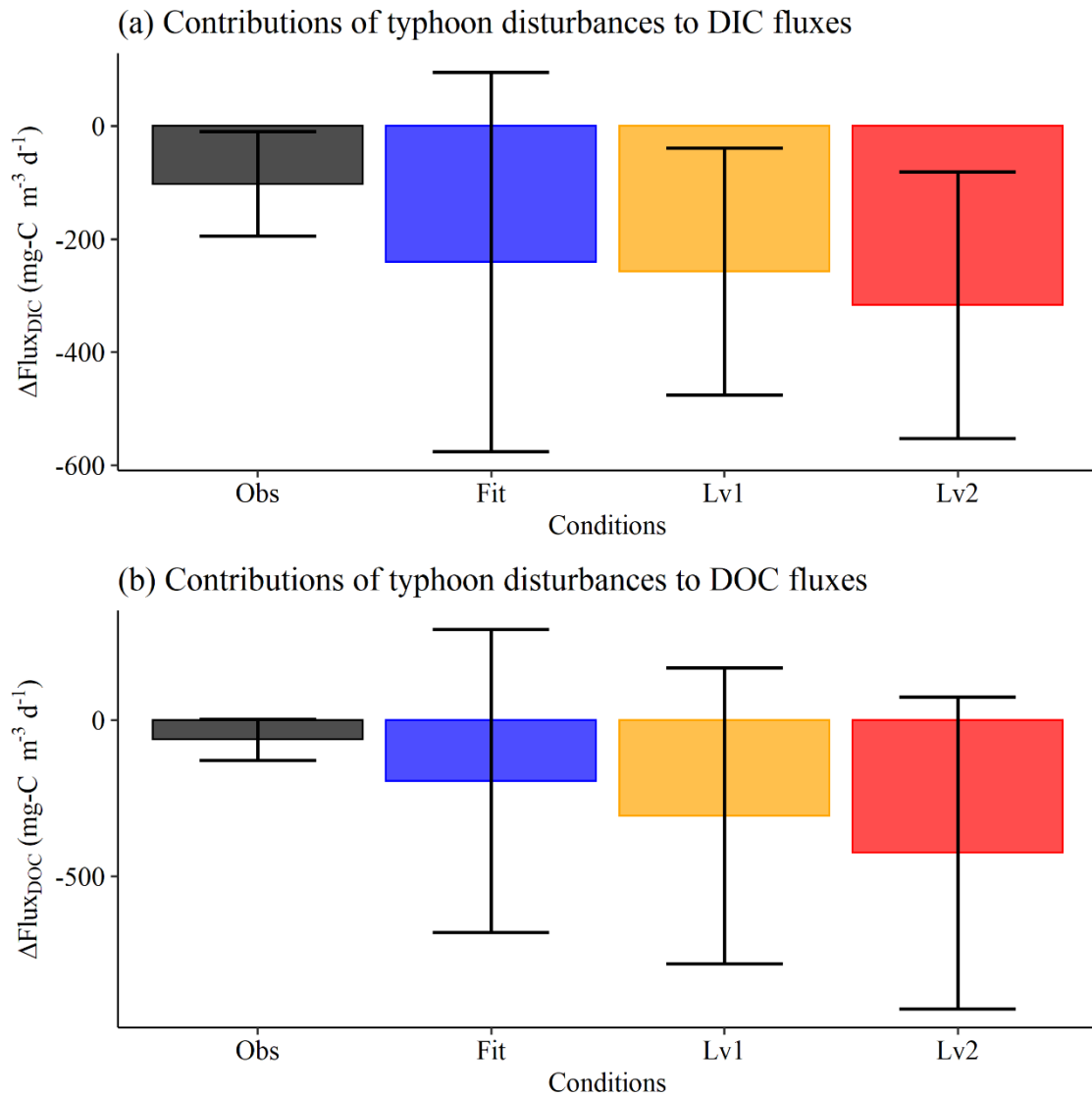
775

776 **Fig. 5.** Continuous daily DIC and DOC data at **(a, c)** upper layer (DIC_U , DOC_U) and **(b,**
777 **d)** lower layer (DIC_L , DOC_L) by using the conceptual equation model under extreme
778 climates from 2015 to 2018. *Blue lines* are original best-fit data, in which the
779 parameters of the DIC model in non-typhoon years are as shown in Table 3, and *gray*
780 *dots* show water sampling (observation) data for each month ($n = 41$) from January
781 2015 to December 2018. *Orange regions* show *Level 1*; *pink regions* show *Level 2*.



782
 783
 784
 785
 786
 787
 788
 789
 790
 791

Fig. 6. Interannual (a) Upper flux_{DIC}, (b) Lower flux_{DIC}, (c) Flux_{DIC}, (d) Upper flux_{DOC}, (e) Lower flux_{DOC}, and (f) Flux_{DOC} ($\text{mg C m}^{-3} \text{d}^{-1}$) grouped by typhoon and non-typhoon years. The *Obs* condition (*black boxes*) show the observation data as in Fig. 5. The *Fit* condition (*blue- boxes*) shows the best-fit data by using the conceptual two-layer carbon model as in Fig.5. *Level 1* (*yellow boxes*) and *Level 2* (*red boxes*) show the extreme scenarios as in Fig. 6. For the definitions of fluxes please see Sect. 2.3.3. Positive values are shown in the carbon sink, and negative ones show the values after carbon was released within YYL.



792

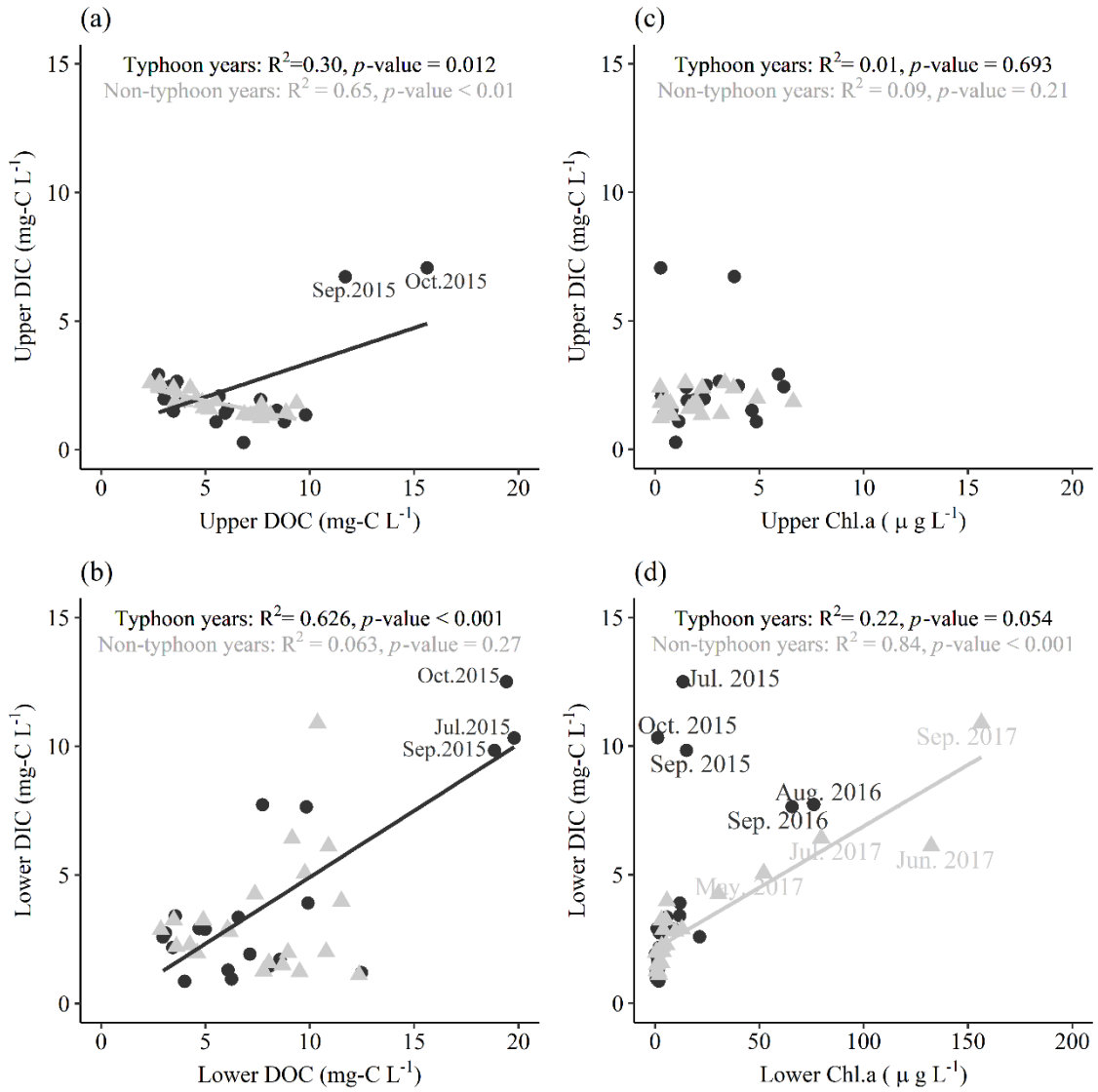
793 Fig. 7. Contributions of typhoon disturbances to (a) DIC and (b) DOC fluxes ($\text{mg-C m}^{-3} \text{d}^{-1}$).

794 Contributions of typhoons to C fluxes ($\Delta\text{Flux}_{\text{DIC}}$, $\Delta\text{Flux}_{\text{DOC}}$) represented the intervals of

795 Flux_{DIC} (or Flux_{DOC}) in typhoon yeas and non-typhoon years (e.g., $\Delta\text{Flux}_{\text{DIC}} = \text{Flux}_{\text{DIC}}$ in

796 typhoon yeas $- \text{Flux}_{\text{DIC}}$ in non-typhoon years).

797



798

799 Fig. 8. Interactions of measurements data in typhoon years and non-typhoon years. The *black*
 800 *circles*: typhoon years, *gray triangles*: non-typhoon years. The solid lines represent the linear
 801 regression line in typhoon years (*black lines*) and non-typhoon years (*gray lines*).

802